

# Atomic force microscopy-based characterization and design of biointerfaces

David Alsteens<sup>1</sup>, Hermann E. Gaub<sup>2</sup>, Richard Newton<sup>3</sup>, Moritz Pfreundschuh<sup>3</sup>, Christoph Gerber<sup>4</sup> and Daniel J. Müller<sup>5</sup>

**Abstract** | Atomic force microscopy (AFM)-based methods have matured into a powerful nanoscopic platform, enabling the characterization of a wide range of biological and synthetic biointerfaces ranging from tissues, cells, membranes, proteins, nucleic acids and functional materials. Although the unprecedented signal-to-noise ratio of AFM enables the imaging of biological interfaces from the cellular to the molecular scale, AFM-based force spectroscopy allows their mechanical, chemical, conductive or electrostatic, and biological properties to be probed. The combination of AFM-based imaging and spectroscopy structurally maps these properties and allows their 3D manipulation with molecular precision. In this Review, we survey basic and advanced AFM-related approaches and evaluate their unique advantages and limitations in imaging, sensing, parameterizing and designing biointerfaces. It is anticipated that in the next decade these AFM-related techniques will have a profound influence on the way researchers view, characterize and construct biointerfaces, thereby helping to solve and address fundamental challenges that cannot be addressed with other techniques.

Surfaces at which tissues, microorganisms, cells, viruses or biomolecules make contact with other natural or synthetic materials are termed biointerfaces. Understanding and manipulating the sensing and interactions that occur at biointerfaces is an enterprise common to a host of scientific fields spanning materials science to medicine, systems to synthetic biology, plant biology to pathology, and oncology to the study of the origins of life<sup>1,2</sup>. Biointerfaces occur between cells and their surroundings, such as the extracellular matrix (ECM), between populations of cells, and between biotic and abiotic elements of engineered systems<sup>3,4</sup>. Biointerfaces are relevant over a wide range of length- and timescales, and their study is amenable to a similarly diverse range of approaches, whether the aim is to dissect fundamental physical and chemical mechanisms, to unravel functional significance or to directly manipulate interfaces.

Our understanding of biointerfaces has been greatly assisted by the development of equipment that probes their structural and functional properties at microscopic, or even nanoscopic, molecular resolution. Powerful techniques have been established that find application in the imaging or characterization of the physical, chemical and biological properties of biointerfaces<sup>5</sup>. However, relatively few methods allow the simultaneous imaging

and multiparametric characterization of biointerfaces in their native state or in an environment that simulates physiological conditions, which is of particular importance to understand how tissues, cells and biomolecules function. Ideally, this information should be provided from the microscopic to the (sub-)nanoscopic scale. Furthermore, it is of great importance to be able to directly modify the morphological, physical, chemical and biological properties of biointerfaces at similar resolution to that at which they can be imaged.

In 1986, atomic force microscopy (AFM) was invented to contour non-conducting solid-state surfaces at atomic resolution by raster scanning a molecularly sharp stylus over the surface<sup>5,6</sup>. Shortly thereafter, researchers began to consider the AFM tip as a nanotool that allows the imaging and manipulation of both living and non-living matter from the atomic to the microscopic scale<sup>7,8</sup>. The elegant simplicity of AFM allowed users to establish various imaging modes optimized for the surface of tissues, cells, viruses, proteins, nucleic acids and biomaterials<sup>9–12</sup>. In addition, imaging biointerfaces from the microscopic to (sub-)nanoscopic scale at unprecedented signal-to-noise ratio, the AFM can be used to simultaneously quantify and map their physical, chemical or biological properties<sup>13–16</sup>. Examples of multiparametric

<sup>1</sup>Institute of Life Sciences, Université catholique de Louvain, Croix du Sud 4–5, bte L7.07.06., 1348

Louvain-la-Neuve, Belgium.

<sup>2</sup>Applied Physics, Ludwig-Maximilians-Universität Munich, Amalienstrasse 54, 80799 München, Germany.

<sup>3</sup>Department of Biosystems Science and Engineering, Eidgenössische Technische Hochschule (ETH) Zürich, Mattenstrasse 26, 4058 Basel, Switzerland.

<sup>4</sup>Swiss Nanoscience Institute, University of Basel, Klingelbergstrasse 82, 4057 Basel, Switzerland.

Correspondence to D. J. M. [daniel.mueller@bsse.ethz.ch](mailto:daniel.mueller@bsse.ethz.ch)

doi:10.1038/natrevmats.2017.8  
Published online 14 Mar 2017

imaging include measuring the binding of ligands to receptors in real time, assessing the action of antibiotics on bacteria, quantifying interactions between molecules and cell and tissue surfaces, and contouring the free-energy landscape of biomolecular reactions at interfaces<sup>12,16</sup>. Moreover, AFM can be used as a nanoscopic toolbox that brings the molecular and cell biological laboratory to the stylus<sup>17,18</sup> and directs molecular interactions at biointerfaces. The AFM stylus has been used, for example, to build up 3D scaffolds with molecular precision<sup>19,20</sup>, to control and direct enzymatic reactions<sup>21</sup> or cell division<sup>22</sup>, and to sculpt and functionalize biointerfaces<sup>23</sup> used to guide cellular behaviour and tissue formation<sup>3</sup>. Insight and engineering possibilities gleaned from different AFM applications provide complementary perspectives that are vital for building a full understanding of biointerfaces and how to engineer them. Many excellent reviews report the unique possibilities AFM offers to study biological problems. However, so far they are all rather specialized and focus on individual applications. In addition, some of them date back as many as ten or more years. Thus, newcomers and established scientists working on the characterization and design of biointerfaces have to search through these publications to find the information needed. In this Review, we provide an up-to-date overview of the most promising AFM-based techniques that can be used to image and characterize biointerfaces of various origins, report the use of AFM-based biosensors to detect biomolecular reactions in real time, and conclude with AFM-based techniques that allow the spatiotemporal analysis, manipulation and design of biointerfaces.

### Basic principles of AFM imaging

Invented to contour surfaces in air under ambient conditions, AFM uses a cantilever with a molecularly sharp stylus at the free end to raster scan and contour the surface of a sample<sup>6</sup>. Such contouring of a sample, which is always corrugated on the molecular scale, deflects the cantilever and changes the position of a laser beam reflected from the back of the cantilever onto a position-sensitive photodiode (FIG. 1a). This information is read by a feedback system, whereby the vertical distance (height) between the stylus and sample adjusts as a consequence of the force that is measured between them. Height values of the stylus at discrete points in the scan are plotted as a reconstruction of the topography of the sample. The functionality of most biointerfaces is closely related to the hydration state, and thus cantilever holders have been designed to operate AFM in buffer solution, at ambient or elevated (for example, 37 °C for mammalian systems) temperature and, if needed, with CO<sub>2</sub> or humidity control. A challenge in applying AFM to image biointerfaces in their native state is to minimize the force at which the AFM tip interacts with the sample. Proteins can be reversibly deformed at imaging forces >50 pN, but in most cases irreversibly deformed at >>100 pN (REF. 24). Similarly, the soft surfaces of mammalian cells easily deform when subjected to the mechanical forces of the contouring stylus. Consequently, if imaging a living cell at forces >100 pN, the cell-membrane is deformed by

the scanning AFM stylus and the AFM topographs show the underlying rigid cellular architecture onto which the membrane has been pressed. In the early days of AFM, the user had to frequently adjust imaging forces and conditions to avoid the deformation of soft heterogeneous biointerfaces, but modern AFM imaging modes contour biological systems with sufficiently precise force control to avoid sample deformation or destruction<sup>12,16</sup>.

**Observing biomolecular systems at work.** Many AFM imaging modes have been developed. In most of them, the stylus is scanned over a sample while the cantilever height is adjusted to avoid excessive force between the stylus and sample (FIG. 1b). Plotting the height of the cantilever for every pixel scanned results in a topography that can approach (sub-)nanometre resolution for a range of native biological systems, including mammalian and bacterial cells<sup>15</sup>, cellular and synthetic membranes, viruses<sup>25</sup>, fibrils, nucleic acids<sup>26,27</sup>, or water-soluble<sup>28</sup> and membrane<sup>29,30</sup> proteins (FIG. 1c–h). Recording time-lapse topographs allows the molecular machinery of cells to be observed directly at work<sup>24</sup>. Studies report the observation of enzymatic subunits of ATP synthase<sup>31</sup>, communication channels<sup>32</sup>, pore-forming proteins<sup>33,34</sup>, toxins<sup>35</sup>, light-driven proton pumps<sup>36</sup>, potassium channels<sup>37,38</sup>, membrane protein diffusion<sup>39,40</sup> and motor proteins<sup>41</sup> in action. The process of fibrillar<sup>42,43</sup> and filamentous<sup>44,45</sup> growth, and of cellular fibrillogenesis and remodelling of ECM proteins<sup>46,47</sup> have also been recorded in time-lapse topographs. The spatial resolution achieved in these topographs strongly depends on the tip radius, the mechanical properties and roughness of the sample, and the force applied to the AFM stylus.

**Common AFM modes for imaging biointerfaces.** The most commonly used AFM imaging mode is the contact mode, in which a stylus is scanned across a surface while applying a constant force. The physical principle by which it works is analogous to the operation of a record player turntable (FIG. 1a,b). A drawback is that a stylus scanning across a surface can generate lateral forces that, in many cases, are sufficient to deform or displace a soft sample. Considerable expertise is required to mitigate this problem while imaging soft biological samples by contact-mode AFM. Other modes of AFM overcome this problem more easily. Dynamic-mode imaging (also named tapping or oscillation mode) oscillates the cantilever close to its resonance frequency so that the stylus only touches the sample intermittently at the very end of its downward movement (FIG. 1b). Consequently, the lateral force and friction applied during contouring of the sample are minimized. Physical interactions with the sample change both the cantilever amplitude and resonance frequency. In amplitude modulated tapping mode, the feedback loop adjusts the stylus–sample distance to maintain a defined set-point amplitude of cantilever oscillation, which is used to reconstruct the sample topography<sup>9</sup>. The main disadvantage of this mode is that the various sources of stylus–sample interactions that change the cantilever amplitude depend on the structural, mechanical and chemical heterogeneity of

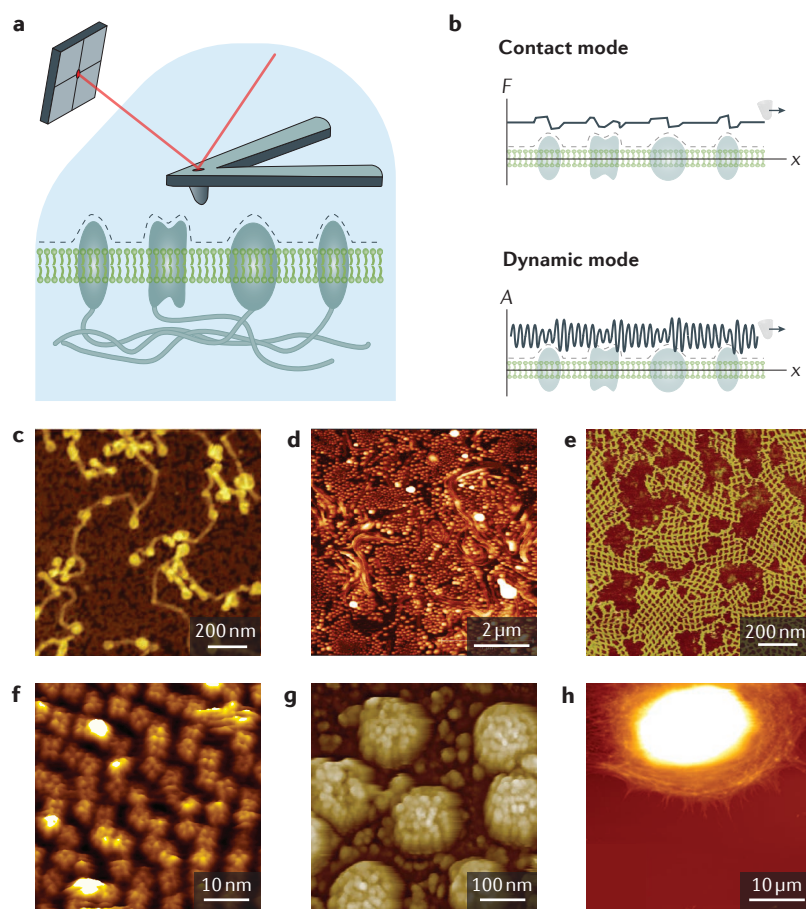


**Figure 1 | AFM imaging principles and applications characterizing biointerfaces.** **a** | Principle of atomic force microscopy (AFM) contouring (dashed line) biointerfaces (an example of a cellular membrane is shown here). The stylus of the cantilever is raster scanned across the sample to record topographic information. Depending on the AFM imaging mode, a feedback loop keeps the force interacting between the stylus and sample at a minimum to prevent distortion of the soft biological sample. **b** | Contact-mode AFM keeps the cantilever deflection constant (constant force) by adjusting the distance between the stylus and sample. Dynamic-mode AFM oscillates the cantilever close to or at resonance frequency, while the stylus only touches the sample surface intermittently. Topographic features affect cantilever oscillation, which is used to adjust the tip-sample distance.  $F$  is force,  $A$  is amplitude and  $x$  is lateral distance. **c** |  $\alpha$ -Synuclein aggregates stimulated by the interaction with phospholipid membranes. **d** | Micellization of phase-separated membrane after exposure to lysine hexachloride dendrimers. **e** | Self-assembly of RNA strands. **f** | MlotiK1 potassium channels. Individual monomers of the tetramers show high structural variability as they can undergo conformational changes that are propagated to the gate of the channel. **g** | Moloney murine leukaemia viruses budding from the surface of an infected 3T3 cell. **h** | Fibroblast grown on a fibronectin-coated substrate. Panel **c** is reproduced with permission from REF. 197, Macmillan Publishers Limited. Panel **d** is reproduced with permission from REF. 198, American Chemical Society. Panel **e** is reproduced with permission from REF. 199, Macmillan Publishers Limited. Panel **f** is reproduced with permission from REF. 37, National Academy of Sciences. Panel **g** is reproduced with permission from REF. 25, American Society for Microbiology. Panel **h** is reproduced with permission from REF. 47, American Society for Microbiology.

the sample<sup>9,48</sup>. Thus, topographs generated by dynamic-mode imaging can consist of a superimposition of surface structure and tip-sample interactions that include stiffness, surface charge, chemistry and friction. The weight of these various contributing elements to such topographs is not always easily deciphered.

**Multifrequency AFM imaging.** More recently, mechanical excitation of the cantilever at several superimposing frequencies has been introduced and broadly termed multifrequency AFM<sup>9</sup>. Multifrequency AFM relies on various approaches, including multiharmonic, bimodal and band excitation<sup>11,49,50</sup>. The imaging process of multifrequency AFM is as fast as that of conventional AFM, and the analysis of multiple cantilever frequencies allows the extraction of multiple properties of a biointerface. However, as a consequence of the conceptual complexity of the multifrequency system, sophisticated theoretical descriptions are required to extract sample properties such as topography, flexibility, adhesion, stiffness and electrostatic potential from observable parameters, such as the amplitude, phase or frequency shifts.

**High-speed AFM imaging.** For a long time, AFM imaging suffered from a rather low time resolution that hindered its capability to follow dynamic processes. Nowadays, key technological advances enable a significant increase in imaging speeds, leading to an operation mode called high-speed AFM<sup>10,51</sup>. These advances include the introduction of small cantilevers with superior response time, the suppression of mechanical vibrations, the development of fast and stable piezo-scanners and the use of a controller that dynamically tunes feedback gains during imaging<sup>10,52</sup>. Nowadays, these improvements make it possible to directly observe chaperones<sup>53</sup>, cytoskeletal motor proteins<sup>41</sup>, light-driven proton pumps<sup>36</sup> and enzymatic rotary motors<sup>31</sup> at work, collagen fibrillogenesis<sup>43</sup> and enzymatic degradation<sup>54</sup>, protein assembly in supported lipid membranes<sup>40,55</sup> and in membranes of living bacteria<sup>56</sup>, and the spatiotemporal dynamics of nuclear pore complexes<sup>57</sup>.

### Molecular and cellular force spectroscopy

**Probing mechanical properties of interfaces.** In the force spectroscopy mode, AFM acts as a versatile toolbox to probe nanomechanical properties and to extract quantitative parameters of biological systems, including from tissues, cells, proteins and nucleic acids, and of non-biological systems, such as functionalized surfaces or matrices. In AFM-based force spectroscopy, a stiff AFM stylus is driven onto a sample and retracted while the force deflecting the cantilever and the distance travelled are recorded in so-called force-distance curves (FIG. 2a). The inter- and intramolecular forces acting on the stylus and biointerface are dependent on their physico-chemical properties and on the buffer solution<sup>58</sup>. Since the early years of AFM, force-distance curves have been used to measure the mechanical properties of interfaces and quantify van der Waals interactions, hydrophobic and -philic properties, charges of ion layers and electrostatic double-layer interactions<sup>13,58</sup>. During approach, the sharp-tipped AFM stylus interacts locally with the biointerface, which it indents until a defined maximum force is reached. Analysis of the approach force-distance curve, and in particular the region describing indentation, allows properties including deformation, elasticity and dissipation to be determined. The retraction curve quantifies the adhesion force between the stylus and sample.

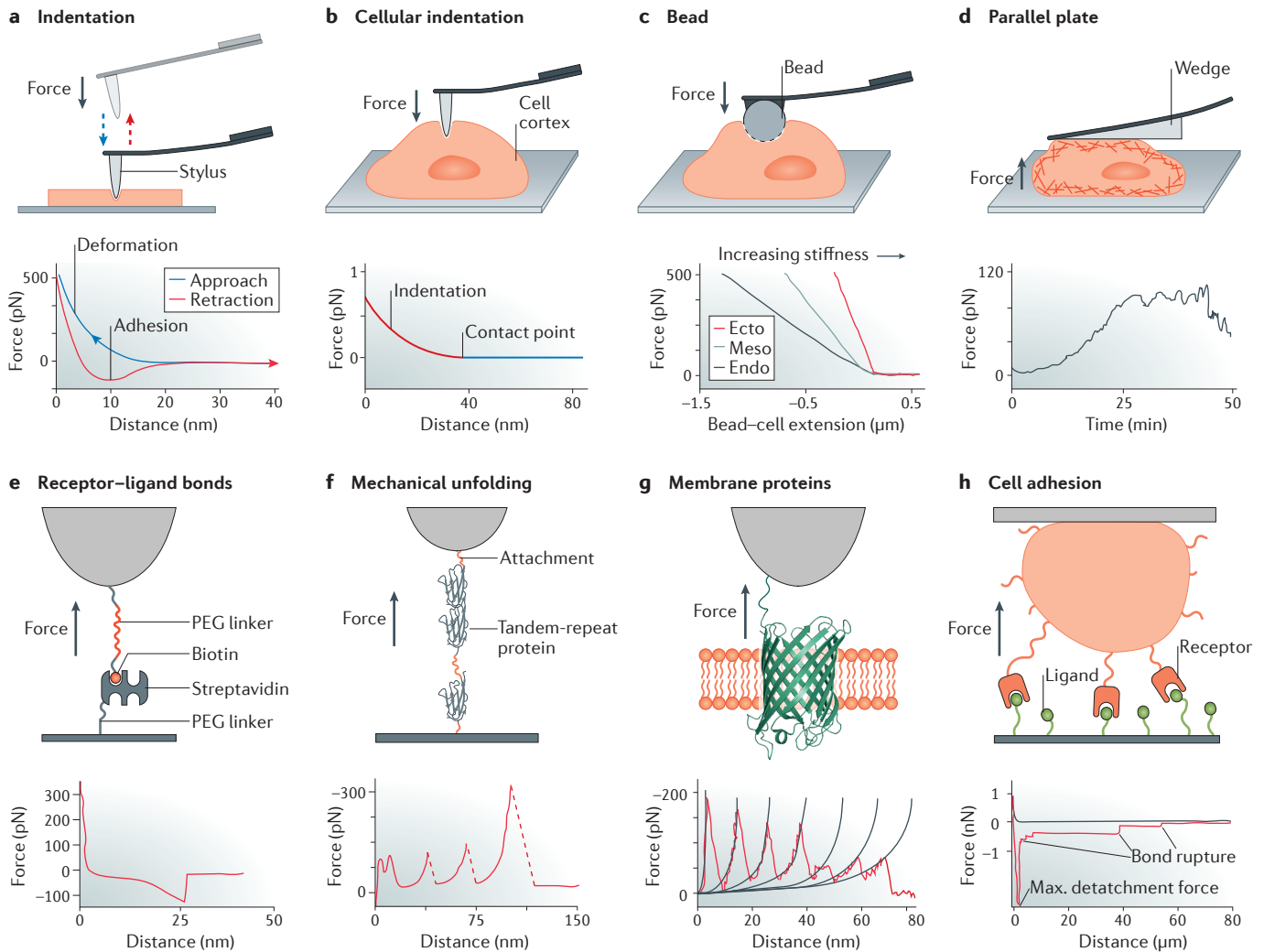


**Figure 2 | AFM-based force spectroscopy from single molecules to cells.** **a** | Force spectroscopy involves an atomic force microscopy (AFM) stylus that indents into and retracts from a sample to locally record interactions and sample properties. Approach and retraction force–distance curves characterize the sample deformation and stylus–sample adhesion, respectively. **b** | Indenting the stylus into a cell locally records mechanical responses by a force–distance curve. **c** | Indenting a bead into a cell probes the mechanical response of larger areas. Force–distance curves show cortical stiffness of ectodermal, mesodermal and endodermal cells of the zebrafish embryo. **d** | Confinement between two parallel plates allows the mechanical response of a cell to be measured. The force–time curve shows the force generated by a HeLa cell progressing through mitosis while confined to a height of 10  $\mu\text{m}$ . **e** | Measuring the strengths of receptor–ligand bonds. Biotin is tethered to the stylus and streptavidin to the support. The force curve recorded upon separating receptor and ligand shows the stretching of the polyethylene glycol (PEG) linker system tethering the proteins and the rupture force of the bond. **f** | Mechanically stretching a tandem-repeat protein. Each force peak characterizes the unfolding of a single protein domain. **g** | Mechanically stressing the terminal end of a transmembrane  $\beta$ -barrel protein leads to the stepwise unfolding of  $\beta$ -hairpins each detected by a force peak. Force peaks of the force–distance curve (red) are fitted by the worm-like-chain model (grey). **h** | Attaching a cell to the cantilever allows cell adhesion to a substrate to be measured. The force–distance curve records the maximal detachment force whereas small force events represent the rupture of single receptor–ligand bonds. Panel **c** is adapted with permission from REF. 63, Macmillan Publishers Limited. Panel **d** is adapted with permission from REF. 123, Macmillan Publishers Limited. Panel **f** is adapted with permission from REF. 98, AAAS. Panel **g** is adapted with permission from REF. 200, Wiley-VCH. Panel **h** is adapted with permission from REF. 114, Elsevier.

Quantification of these mechanical parameters depends on the contact area of the stylus and sample, which with a soft interface, such as a cell or polymer cushion, increases non-linearly with indentation depth and is difficult to determine. To circumvent this problem, either the depth of indentation can be limited so that only the very tip of the stylus interacts with the sample

or a nano- or micrometre-scale bead can be attached to the end of the cantilever, which allows for a more accurate estimation of contact area and sample indentation<sup>59</sup> (FIG. 2b,c). Force spectroscopy has enabled the characterization of the mechanical properties of living cells, and has allowed these properties to be correlated with nanomechanical activity<sup>60</sup>, touch sensation<sup>61,62</sup>,

development<sup>63,64</sup>, cell states in mitosis<sup>65,66</sup> and cancer<sup>67,68</sup>. AFM imaging and force spectroscopy have also been combined to characterize the mechanical properties of viruses depending on the packing of nucleic acids, on capsid proteins or on environmental conditions<sup>69–71</sup>. Although such approaches open promising avenues towards characterizing the mechanical properties of biological systems, the mechanical response of these systems depends on the speed of indentation (that is, the loading rate at which force is applied)<sup>72,73</sup>. Because this mechanical response to the indentation speed is non-linear and varies between biological systems, extrapolation from a single loading rate is not recommended. Thus, to understand the mechanical properties of a biological system, the characterization of this response over a wide range of loading rates is required<sup>61,74,75</sup>.

Matters are further complicated by the heterogeneous nature of biointerfaces, including tissues, cells, cellular membranes, proteins or biomacromolecules. In such cases, the location at which the stylus indents the biointerface is relevant. Therefore, heterogeneous samples are best described by a series of spatially resolved force–distance curves (see ‘Imaging and multiparametric characterization’). Another approach is to confine a rounded living cell between two parallel plates: a wedged AFM cantilever and the substrate supporting the cell<sup>22,76</sup> (FIG. 2d). In a confined cell, the interplay between cell cortex tension and pressure can be described by the Laplace law<sup>77</sup>, allowing rheological measurements<sup>78</sup>.

**Single-molecule force spectroscopy of bonds.** Single-molecule force spectroscopy (SMFS) is frequently applied to detect the binding strength of ligand receptor pairs. To do so, a receptor or ligand is tethered to the AFM stylus and the cognate ligand or receptor to a surface support. Bringing the stylus and support into proximity allows a ligand–receptor bond to form, and subsequent retraction of the stylus forces the bond to rupture (FIG. 2e). The strength of the receptor–ligand bond can be inferred from such rupture forces recorded in the force–distance curve. Originally applied to measure the force required to unbind streptavidin and biotin<sup>79–81</sup>, it was quickly recognized that measuring rupture forces at different separation speeds (that is, loading rates) provides information about the kinetic properties of a bond<sup>80</sup>. Probabilistic modelling of bond dynamics<sup>82–84</sup> can be applied to estimate the thermodynamic and kinetic properties of ligand–receptor bonds. These properties include the free energy difference,  $\Delta G_u$ , between the bound and transition state or unbound state; the distance,  $x_u$ , between the bond and transition state; and the transition rate of the bond,  $\tau_u$  (reciprocal of lifetime  $t_u$ ). The lifetime of molecular bonds can be also measured by subjecting the bond to a low constant force and waiting for the rupture of the bond<sup>85,86</sup>. Constant forces can be applied (for example, clamped) artificially by the AFM feedback system<sup>87,88</sup> or naturally by cell membrane tethers<sup>89</sup>. Energetic properties of bonds characterized by SMFS include ligands binding to G-protein-coupled<sup>90</sup> or serotonin<sup>91</sup> receptors, cell adhesion to ECM substrates<sup>92</sup>, scaffold stability of bacterial cellulosomes<sup>93</sup> and viruses binding to cell surface receptors<sup>94,95</sup>. To accurately

extrapolate the thermodynamic properties of biomolecular interactions requires probing at very slow speeds and high force sensitivity. The Perkins group established an ultrastable AFM that reduces drift to 100 pm over tens of minutes<sup>96</sup> and sculpted AFM cantilevers using a focused ion beam (FIB) to approach sub-piconewton resolution<sup>97</sup>. Such ultrastable and sensitive AFM assays are likely to become more important to probe interaction strengths and landscapes of biointerfaces in greater detail.

**Protein stability and folding at interfaces.** 20 years ago it was demonstrated that individual domains of the giant muscle protein titin can be mechanically unfolded by SMFS and can be refolded on relaxation<sup>98</sup> (FIG. 2f). This experiment inspired researchers to characterize the structural stability and the unfolding, misfolding and refolding pathways of various proteins<sup>99–101</sup>. With such SMFS-based assays, the effect of mutations<sup>102</sup>, external agents, such as chaperones<sup>103,104</sup>, or other co-factors<sup>21,86,105</sup> on protein stability and folding pathways become accessible. It has been observed that pulling one terminal end of a membrane protein induces the stepwise unfolding and extraction of secondary structural elements from the membrane<sup>106,107</sup> (FIG. 2g). Although small partially unfolded membrane proteins can refold from the aqueous phase into the membrane<sup>107,108</sup>, large proteins are typically too complex and misfold<sup>109,110</sup>. However, in the presence of chaperones or translocons/insertases, large unfolded membrane proteins can insert and refold secondary structures stepwise into the membrane until the protein achieves its native structure<sup>110,111</sup>. Moreover, because SMFS applied to membrane proteins detects the stability of secondary structure elements and polypeptide loops, it can be applied to study in great detail how functional state, lipid composition or mutations affect protein structure<sup>99</sup>.

One limitation of SMFS is the low experimental throughput, a natural consequence of most single-molecule approaches. Efforts to overcome this limitation have taken various forms. One is the automation of SMFS experiments, which must be achieved while retaining control of the experimental conditions (for example, buffer, temperature, cantilever calibration and drift)<sup>112</sup>. A recent development of a microfluidic platform, in which 640 spots of different proteins are covalently anchored to a coverslip and each protein is mechanically phenotyped by automated SMFS<sup>113</sup>, is indicative of the potential of this approach.

**Quantifying cell adhesion to interfaces.** Single-cell force spectroscopy (SCFS) measures the adhesion of a single cell to a biointerface, which can be tissue, another cell or a surface functionalized with ligands<sup>15,114</sup>. In most cases, SCFS uses an AFM compatible with modern light microscopy and is operated under conditions that are physiologically relevant for mammalian or bacterial cells. A single cell is then attached to the free end of a tiptless cantilever. To facilitate this attachment the cantilever can be functionalized with charged or hydrophobic polymers (such as polyethyleneimine, poly-L-lysine or polydopamine) or with receptors (such as concanavalin A) that bind sugar residues at the cell surface<sup>114</sup>. Guided by optical

microscopy, the functionalized cantilever is lowered into contact with a trypaninized cell, which readily attaches to the cantilever. After this, the probe cell is brought into contact with a biointerface for a given contact time and force, and then withdrawn while a force–distance curve is recorded (FIG. 2 h). Analysis of the force curve provides the maximum adhesion force of the cell, which on separation quickly decays in discrete steps. These steps describe the rupture of bonds formed between cell surface receptors and ligands<sup>114</sup>. This approach allows, for example, assaying how cells strengthen adhesion to ECM proteins or other substrates. Examples that have been characterized are *Dictyostelium discoideum* forming adhesion<sup>115</sup>, integrins initiating cell adhesion to ECM proteins<sup>92</sup>, cadherins forming cell–cell adhesion<sup>116</sup>, activated leukocyte cell adhesion molecules (ALCAMs) forming T cell contacts<sup>117</sup>, and bacteria and yeast adhering to interfaces<sup>118,119</sup>. Because the cell adheres to the cantilever, this interface can also be treated to stimulate cell surface receptors and probe how this influences the cell to initiate and strengthen adhesion to another substrate<sup>120</sup>.

SCFS is frequently combined with optical microscopy to monitor cell morphology during an adhesion experiment or to localize fluorescently labelled proteins<sup>15</sup>. The cell morphology changing in response to mechanical forces can be well observed in 3D by confocal or spinning disk confocal microscopy. Alternatively, different solutions for side-view imaging have been developed, allowing the direct observation of cantilever, cell and substrate<sup>121,122</sup>. Such combinations have been applied to investigate mechanical processes in cells inducing membrane bleb formation or actomyosin cortex assembly<sup>66,122,123</sup>. Other experiments have characterized the role of the actomyosin cortex and cell membrane in membrane tether extraction<sup>89,117,124</sup>.

### Imaging and multiparametric characterization

The combination of AFM imaging and force spectroscopy has created new possibilities for the multiparametric investigation of biological samples<sup>11,16</sup>. The combination of modes is frequently referred to by one of several brand names. Brands developed by different companies differ in how they move the stylus and sample in relation to one another to record force–distance curves. However, we refer to all such modes by the general name of force–distance curve-based (FD-based) AFM. FD-based AFM records at least one force–distance curve for each pixel of the resulting topography by approaching and retracting the stylus to and from the sample, respectively. The relative ease of interpreting force–distance curves (see above sections on force spectroscopy) allows the straightforward extraction of mechanical parameters such as sample deformation, elasticity and stiffness (FIG. 3). Examples of imaging and mapping of mechanical properties of biointerfaces include the furrow stiffening of dividing animal cells<sup>65</sup>, various animal and bacterial cells<sup>125–128</sup>, viruses<sup>71</sup>, membranes and membrane proteins<sup>74,129,130</sup>, and amyloid fibrils<sup>131,132</sup>.

As introduced in the example of SMFS, functionalization of the AFM stylus with chemical groups, ligands, receptors or viruses allows the detection of specific interactions with biointerfaces and, for FD-based AFM,

the ability to spatially map these interactions to the sample topography (FIG. 4). Examples include mapping of chemical groups, sugars or proteins on animal and bacterial cell surfaces<sup>133–135</sup>, electrostatic properties of membranes<sup>74,136</sup> and membrane proteins<sup>137</sup>, bacteriophages extruding from bacteria<sup>138</sup>, enveloped viruses binding to surface receptors of animal cells<sup>95</sup> and ligands binding to human G-protein-coupled receptors<sup>90</sup>. The binding of two ligands to the same receptor<sup>139</sup> and high-resolution (~2–5 nm) mapping of ligand-binding events on larger protein complexes<sup>140,141</sup> have also been demonstrated.

FD-based AFM records hundreds of thousands of force–distance curves per topograph to map mechanical properties and/or interactions. Commercially available AFMs require tens of minutes to record this amount of data. Thus, rapid measurements are desirable to reduce the image acquisition time and to enable the mapping of dynamic biological processes. The first attempt to bring SMFS to the previously unexplored microsecond time-scale was achieved by torsionally oscillating T-shaped cantilevers at high frequency<sup>129</sup>. This innovative concept considerably reduced the recording time of topographs and multiparametric maps<sup>141,142</sup>. However, the faster ligand–receptor bonds or chemical interactions are ruptured the more they are forced out of equilibrium. The more a system is forced out of equilibrium the more difficult it is to extrapolate its equilibrium behaviour<sup>82–84</sup>. Thus, mapping chemical interactions close to thermal equilibrium requires separating the interactions slowly. In addition, some bonds, such as catch-bonds, show biphasic responses to separation speed, and therefore cannot be described using a limited range of loading rates<sup>143</sup>. Currently, probing such biomolecular interactions over a wide range of loading rates is time consuming, because different rates must be sequentially probed one after the other. Therefore, it seems possible that alternative ways to speed up the data acquisition process over a large range of loading rates will have to be developed. At high pulling speeds (that is, high loading rates), the hydrodynamic drag<sup>144</sup> and physical limitations<sup>58,145</sup> of the cantilever must be considered to correctly analyse the biomolecular interactions probed. Recent attempts have seen fast FD-based AFM approaches applied to automatically probe biomolecular interactions at low to very high loading rates from ~10<sup>3</sup> to 10<sup>6</sup> pN s<sup>-1</sup> (REFS 90,142). It might be expected that ultrastable AFMs<sup>96,97</sup> combined with further improved high-speed force spectroscopy approaches<sup>142,146</sup> will soon extend this range of loading rates to characterize biointerfaces.

### Microcantilever-based sensors

Another broad area of application of AFM is the use of microcantilever arrays to sense chemical and biological interactions and processes<sup>17</sup> (FIG. 5a). Adsorption of molecules on to cantilevers changes the mass and resonance frequency (dynamic mode) of the cantilever or induces surface stress that deflects the cantilever (static mode). Thus, by functionalizing one cantilever surface with a chemical or biological compound and passivating the remainder to suppress unspecific interactions, it is possible to detect specific interactions of molecules or cells

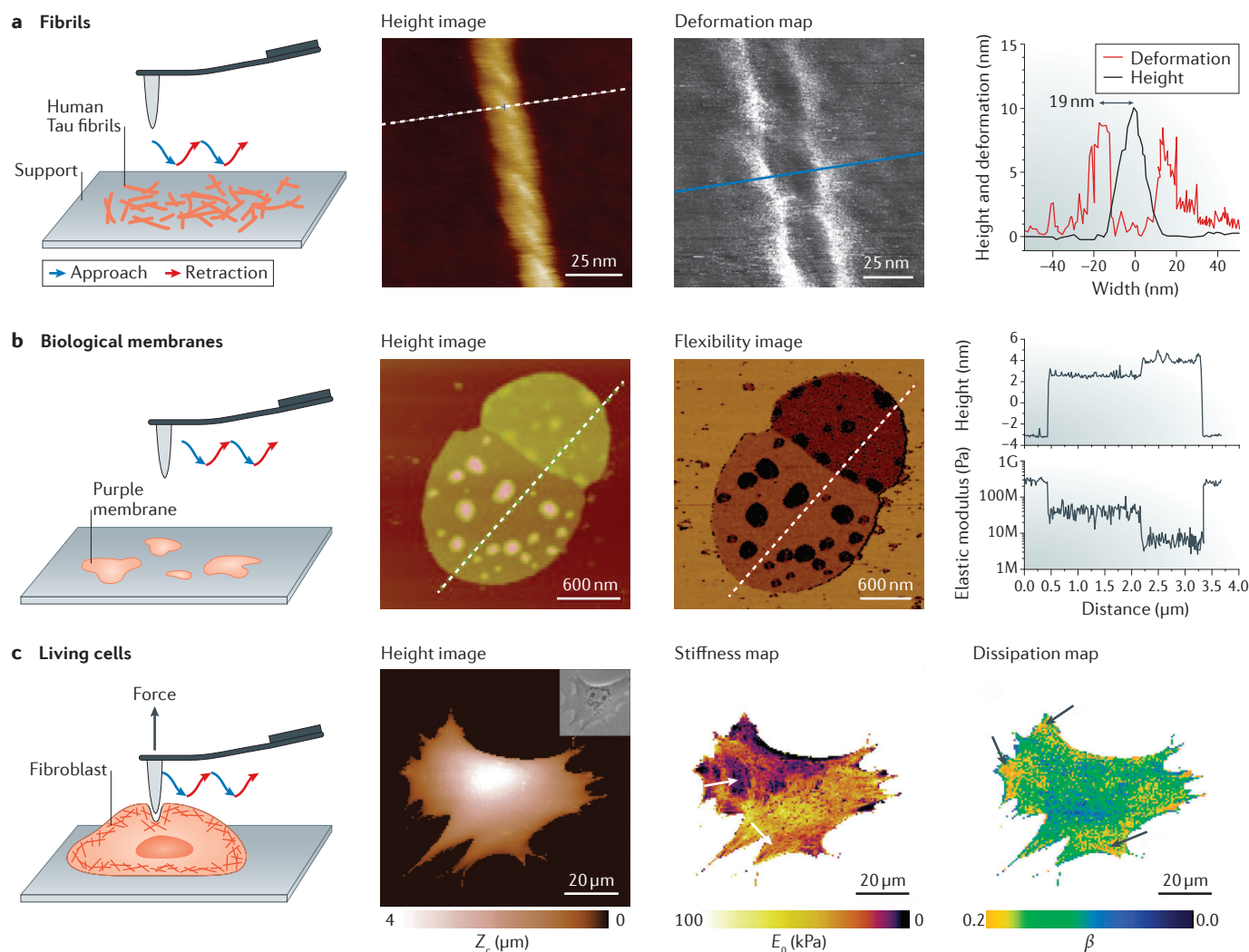


**Figure 3 | AFM-based imaging and mapping of mechanical properties of biointerfaces.** **a** | High-resolution mechanical analysis of a human pathological amyloid-like Tau fibril. The height image, deformation map and cross-section analysis correlate the height (black) and deformation (red) of a fuzzy coat surrounding the fibrillar core. **b** | Height and flexibility map and profiles recorded of native purple membrane surfaces, of lipids and of the membrane protein bacteriorhodopsin. The measurements differentiate the stiffness of purple membrane surfaces. **c** | Height image, stiffness map and dissipation map of a live mouse embryonic fibroblast correlate stiff fibrous structures, which are most likely cytoskeletal fibres (white arrows), and cellular areas dissipating mechanical energy (grey arrows).  $\beta$ , power law exponential;  $E_0$ , modulus scaling parameter;  $Z_c$ , contact height. Panel **a** is adapted with permission from REF. 131, National Academy of Sciences. Panel **b** is adapted with permission from REF. 129, Macmillan Publishers Limited. Panel **c** is adapted with permission from REF. 126, Royal Society of Chemistry.

with the functionalized interface (FIG. 5b). Experiments with such cantilevers have allowed the specific binding of biomolecules that include DNA, proteins<sup>147-149</sup>, bacteriophages and cellular membranes<sup>150</sup>, peptides and antibodies<sup>151,152</sup>, enabling the study of physiologically relevant conditions. Because the binding of biomolecules to the biointerface directly affects the cantilever motion, binding can be detected in real-time with pico- or even femtomolar sensitivity<sup>150</sup>. For analysis in daily laboratory routines, procedures have been developed to coat individual cantilevers in an array with functionalizing solutions using micropipettes or inkjet spotters<sup>17</sup>. Various procedures have been developed to improve the sampling rate and sensitivity of detection of cantilever deflection and thus improve assays that sense binding to interfaces.

Assessing the eligibility of patients for cancer treatment by genetic markers has led to numerous targeted therapy approaches. In malignant melanoma, the deadliest form of skin cancer, 50% of all cases carry the mutation V600E in the *BRAF* gene encoding the serine/threonine-protein kinase B-raf<sup>153</sup>. To assess treatment efficacy, cantilever array sensors have been applied in a clinical trial<sup>154</sup> to identify mutations in the *BRAF* gene from human biopsies with single point mutation sensitivity and without the need for sequencing or labelling (FIG. 5c,d). The cantilever assay shortens processing time to a few hours compared with current technologies, such as Sanger and next-generation sequencing methods<sup>154</sup>. In other examples, microcantilever arrays have been applied to characterize mammalian cells and bacteria<sup>155</sup> and the interaction of

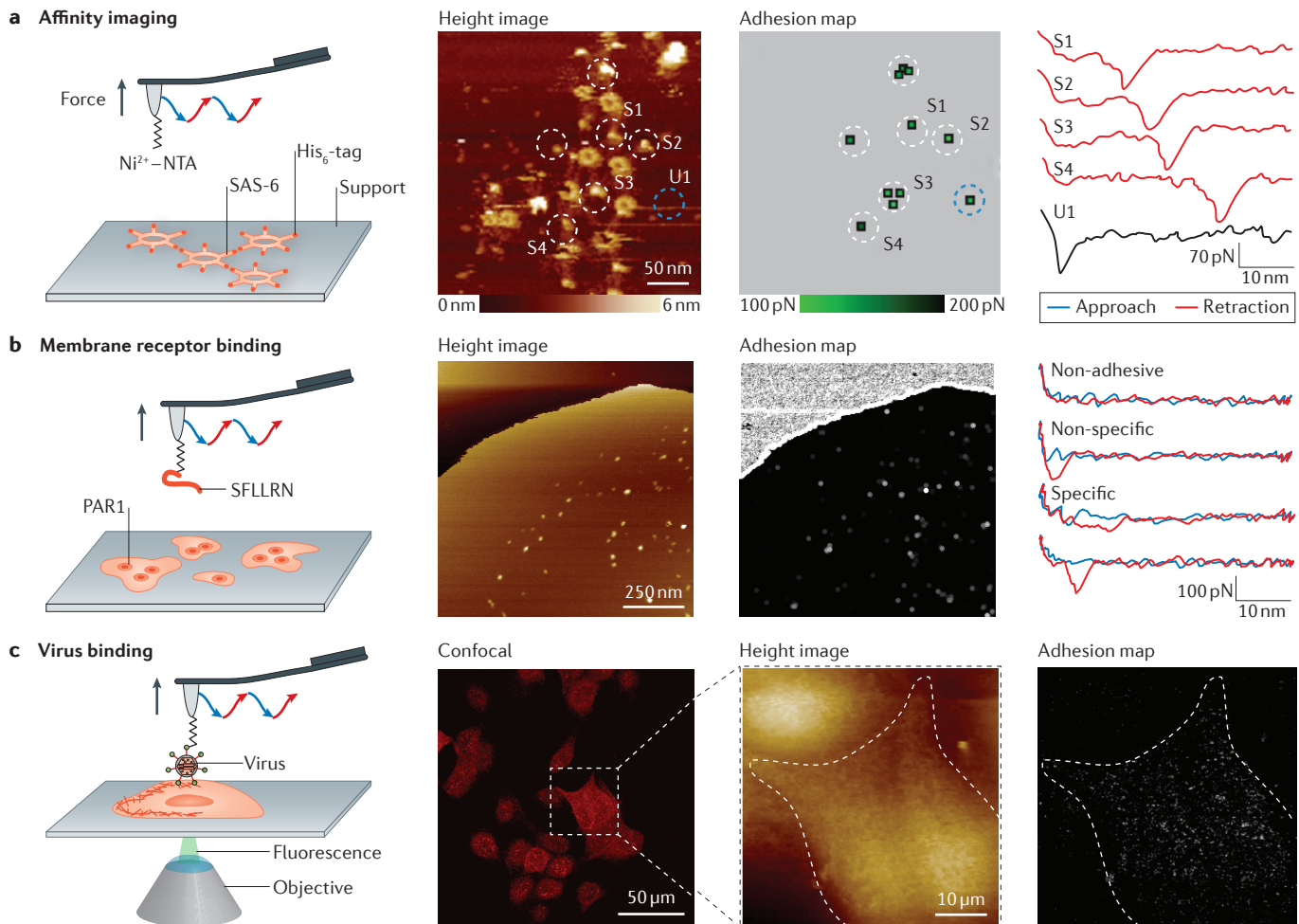


**Figure 4 | AFM-based imaging and affinity mapping of biointerfaces.** **a** | High-resolution affinity imaging of the spindle assembly abnormal protein six homologue (SAS-6) using a Ni<sup>2+</sup>-N-nitrilotriacetate (Ni<sup>2+</sup>-NTA) functionalized atomic force microscopy (AFM) stylus. Topography and corresponding adhesion map correlate the specific (S) adhesion events encircled in white to the emanating arms of SAS-6. Unspecific (U) adhesion events are encircled in blue. Force–distance curves show selected specific and unspecific events. **b** | Mapping ligand binding to human protease activated receptor 1 (PAR1) using a stylus functionalized with the native SFLLRN-peptide ligand. Topography (height image) and adhesion map together with the force–distance curves show specific binding events that occur only at receptors. **c** | Mapping of virus-binding events on living MDCK cells. The MDCK cells either express TVA receptors (red) or not. An AFM stylus bearing a single EnvA-pseudotyped rabies virus is used to image and map the virus-binding sites on cells. Topography and adhesion map were recorded of the area selected (enclosed in a white frame in the confocal image), including fluorescent and non-fluorescent cells. Only cells expressing the receptors show specific binding events of the virus (framed by white dashed lines). Panel **a** is adapted with permission from REF. 140, American Chemical Society. Panel **b** is adapted with permission from REF. 90, Macmillan Publishers Limited. Panel **c** is adapted with permission from REF. 95, Macmillan Publishers Limited.

bacteria with antibiotics. Although live bacteria induce nanometre-scale fluctuations in the motion of cantilevers to which they are attached, dead ones do not<sup>156</sup> (FIG. 5e). Such applications provide fast and reliable diagnostics in the battle against multiresistant bacteria and help to quickly identify appropriate therapies for patients<sup>151,152,156</sup>.

**Patterning and assembly of biointerfaces**

*Assays for the assembly of molecular systems.* Progress in biointerface research and application depends on the ability to characterize and engineer them<sup>1,2</sup>. AFM is suited not only to imaging interfaces at the (sub-)nanometre scale, but also to manipulating surfaces, because AFM operates with a stylus in close proximity to or in contact

with a sample. Scanning probe nanolithography (SPL) encompasses various approaches that either remove or add material with nanometre precision and relatively modest technological demands<sup>20,157</sup> (FIG. 6). The range of SPL approaches stems from the wealth of nanoscale interactions that can be manipulated by an AFM stylus. Such interactions can be mechanical, thermal, electrostatic or chemical in nature, or combinations thereof. Recent developments allow SPL to be performed in ambient atmosphere or in buffer solution, which allows manipulation of soft matter such as organic molecules, polymers and proteins<sup>158,159</sup>. These capabilities make SPL appealing for research and engineering applications of biointerfaces. Although numerous promising AFM-based

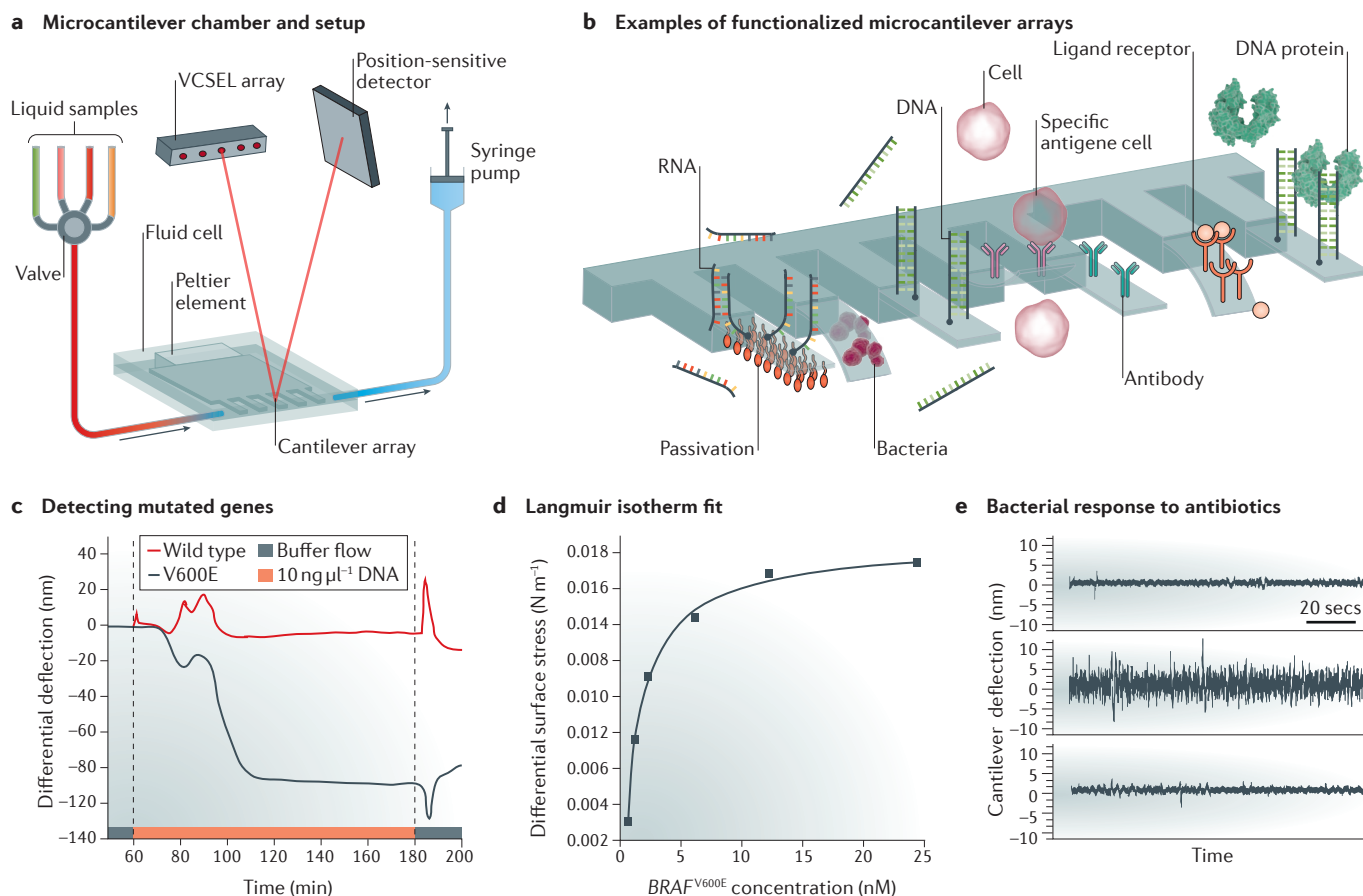


**Figure 5 | Characterizing reactions of biointerfaces in real time using AFM-based microsensors.** **a** | Environmental chamber of a microcantilever array. The Peltier element controls the temperature, and input and output tubes exchange liquids. Laser beams are reflected from microcantilevers onto a position-sensitive detector to measure their motions. **b** | Principle of microcantilever arrays detecting biomolecular and cellular interactions. Individual microcantilevers are functionalized with chemical or biological molecules or cells to detect their interactions by the differential readout of their deflection. Examples include functionalization with RNA, DNA, antibodies or cells. Passivation prevents non-specific interactions of solutes with the cantilevers. **c** | Surface stress of microcantilevers functionalized with the V600E mutated *BRAF* gene and measured after injection of a solution containing a wild type (red) and mutant *BRAF*<sup>V600E</sup> gene (grey). Dashed lines and coloured bars indicate the duration of solution injection. **d** | Langmuir isotherm ( $R^2 = 0.97$ ) fit of experimental data showing that the 13-mer *BRAF*<sup>V600E</sup> sequence can be detected in a larger DNA fragment at various concentrations. **e** | Probing bacterial vibrations at the nanometre scale and the action of antibiotics. The top section shows cantilever fluctuations before attachment of bacteria; the middle section shows that attachment of bacteria increases the mechanical fluctuations of the cantilever; and the bottom section shows that fluctuations cease upon exposure to antibiotics. Panels **b–d** are adapted with permission from REF. 153, Macmillan Publishers Limited. Panel **e** is adapted with permission from REF. 156, National Academy of Sciences.

applications have been introduced to pattern and assemble biointerfaces hierarchically, we focus here on a few advanced examples that remove, modify or deposit material on surfaces. These include mechanical SPL, thermal and thermochemical SPL (t-SPL and tc-SPL), dip-pen nanolithography (DPN) and single-molecule cut-and-paste (SMCP).

Most SPL applications sculpt nanoscopic patterns by depositing or removing layers of macromolecules onto a surface<sup>20</sup> (FIG. 6a). The patterning of block copolymers<sup>160</sup>, lipids<sup>161</sup>, collagen matrices<sup>158,162</sup> and proteins<sup>158</sup> have been reported. Currently, the throughput of patterning a surface with 10 nm precision using a single AFM stylus approaches the range of  $10^4$ – $10^5$   $\mu\text{m}^2\text{h}^{-1}$ . Nowadays, the combination of non-destructive AFM imaging and the

patterning of interfaces enable automatized closed-loop lithography. Such lithography tools can autonomously image, pattern and optimize the patterning process<sup>20</sup>, facilitating the creation of high-resolution nanoscale structures.

**Thermal scanning probe lithography.** Organic polymers are used for resists in optical lithography or to design nano- and microscopic devices (for example, polydimethylsiloxane masks) for biological research. In t-SPL, an AFM stylus is heated to 300–350 °C in  $\sim 5.5$   $\mu\text{s}$  pulses to locally desorb material from a thin organic film<sup>19</sup> (FIG. 6c,d). 2D patterns can be freely shaped with the precision of a few nanometres (FIG. 6e). 3D structures can be sculpted using this technique by the successive

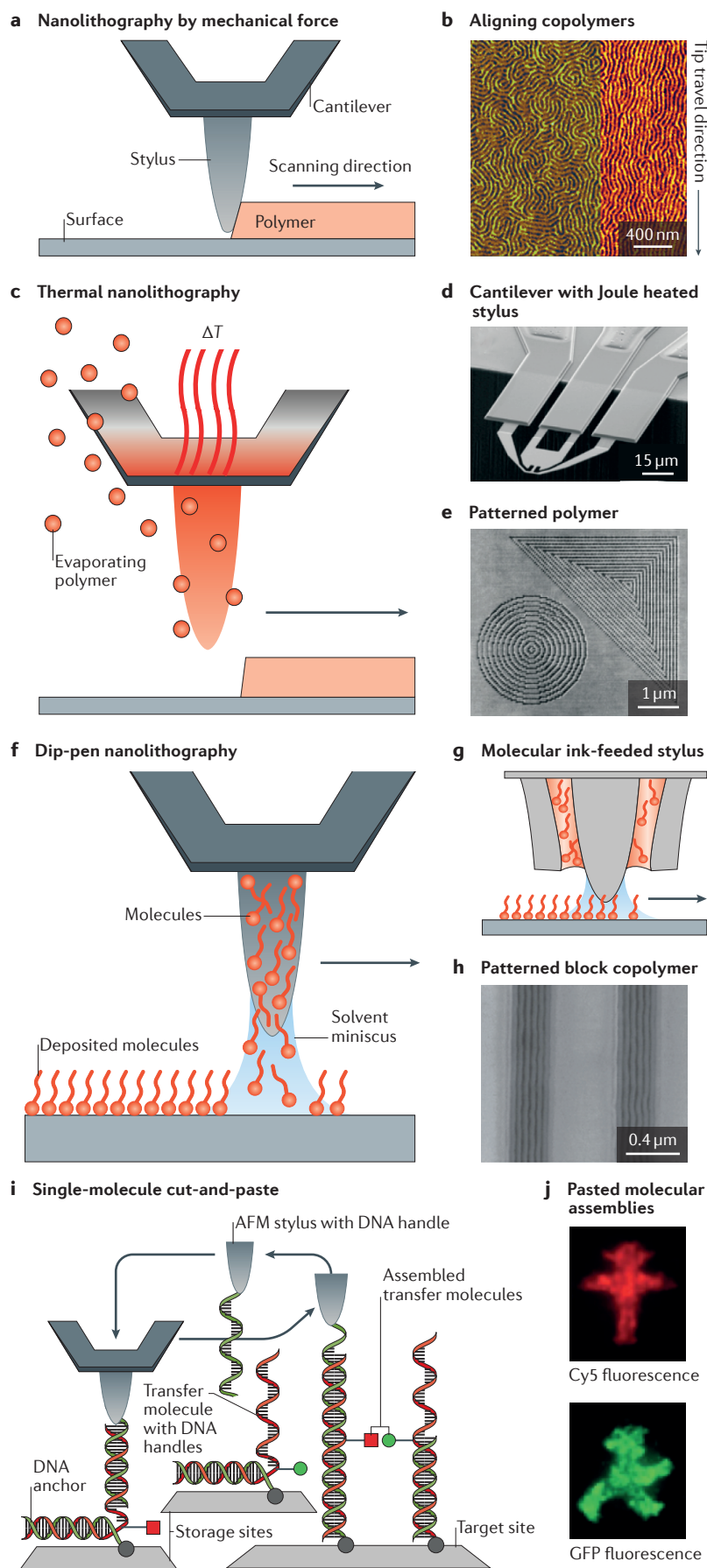


**Figure 6 | AFM-based sculpting, patterning and assembly of biointerfaces.** **a** | Principle of scanning probe lithography (SPL). By adjusting the force applied to the atomic force microscopy (AFM) stylus, thin layers deposited on surfaces are patterned with nanometre precision. **b** | Stylus-aligned region of copolymer chains coating a surface. **c** | Principle of thermal SPL. **d** | Scanning electron microscopy (SEM) of a silicon cantilever comprising integrated joule heaters for tip heating to evaporate molecular resists coating an interface. **e** | Topograph of a nanoscopic pattern written into phthalaldehyde polymer in 0.76 seconds. **f** | Principle of dip-pen nanolithography. An alkanethiol ink-coated AFM stylus brought into contact with a gold substrate forms a water meniscus (blue) through which molecules diffuse to the surface. While scanning, ink molecules assemble along the path of the stylus, forming stable nanostructures. **g** | Patterning using a hollow stylus that feeds molecular ink from a reservoir to the support. **h** | SEM showing patterned PS-*b*-PMMA block copolymers (depth 70 nm, width 260 nm). **i** | Principle of the single-molecule cut-and-paste (SMCP) process. The AFM stylus uses a DNA oligomer to pick up single molecules from discrete storage sites and transfer them to a target site, where they are deposited with nanometre precision. The length and binding geometry of DNA oligomers used as an anchor or handle are chosen such that this process can be repeated many thousands of times. **j** | Pedestrian traffic light icons assembled from proteins with red (Cy5) and green (GFP) fluorophores by SMCP. The height of the icons is approximately 7.5 μm. PMMA, polymethyl methacrylate; PS, polystyrene. Panels **d** and **e** are reproduced with permission from REF. 164, Institute of Physics. Panels **f** and **g** are adapted with permission from REF. 169, Macmillan Publishers Limited. Panel **h** is reproduced with permission from REF. 172, Macmillan Publishers Limited. Panel **i** is adapted with permission from REF. 23, AAAS. Panel **j** is reproduced with permission from REF. 201, American Chemical Society.

removal of material in layers of defined thickness. Recent improvements of the technique have considerably shortened turnaround time, and surfaces can be structured with a line frequency of up to 500 kHz (REFS 163,164). Other developments include the use of heated styluses to locally remove covalently bound material<sup>165,166</sup> or to induce chemical modifications (such as in tc-SPL)<sup>163,167</sup>. The ability to directly create structures on interfaces and to chemically modify them provides opportunities for innovative biointerface research and engineering<sup>157</sup>.

**Dip-pen nanolithography.** DPN uses an ‘ink’-coated AFM stylus to deliver molecules to a surface through a solvent meniscus, which forms in ambient atmosphere by capillary condensation<sup>168,169</sup> (FIG. 6f). This direct-write technique offers high-resolution patterning capabilities for several molecular and biomolecular inks on a range of hard- and soft-matter substrates, such as metals, semiconductors, glass and functionalized surfaces. An ink is a solution of molecular compounds to be deposited by DPN. Water-insoluble inks, such as solvent-free preparations of phospholipids, can also be deposited to a surface in an aqueous environment via the meniscus that

forms between the immiscible ink and water<sup>170</sup>. Owing to the capability of directly writing multiple compounds sequentially by dipping a stylus into a reservoir of one ink after another, or in parallel by using multiple styluses writing in different inks, DPN is an appealing tool for depositing molecules with nanoscopic precision. Alternatively, nanodispensing approaches use hollow styluses with an annular aperture to deposit ink<sup>171</sup> (FIG. 6g). The patterning of interfaces with nanoarrays of biological or organic molecules is of particular interest in biointerface research, because these arrays can be used to direct cellular processes including adhesion, migration and proliferation. Notably, a range of macromolecules, including DNA, peptides, proteins, block copolymers, lipids, as well as viruses and bacteria, have been patterned using direct-write or indirect adsorption approaches<sup>169,172</sup> (FIG. 6h). The conceptual simplicity of AFM lends itself to parallelization using cantilever arrays<sup>173</sup>. However, because using several AFM styluses in parallel is not suitable for large-scale molecular printing or massive parallelization, 2D arrays of styluses have been introduced with as many as 55,000 styluses that can write molecular patterns on surfaces simultaneously<sup>174</sup>. Such 2D arrays of styluses increase the throughput of DPN by orders of magnitude and allow the processing of centimetre-scale surfaces with <100 nm precision. In the meantime, DPN arrays have been engineered with even more styluses to pattern interfaces with biological molecules<sup>157</sup>.

**Single-molecule cut-and-paste.** SMCP combines the superb positioning precision of AFM with the selectivity of biomolecular recognition to pick individual molecules from a depot chip and arrange them on a target interface one by one<sup>23</sup> (FIG. 6i). Functional molecular ensembles are created bottom-up on the target interface with properties arising from the composition and arrangement of their constituent molecules. A molecular assembly is created by allowing a functionalized AFM stylus to bind to a transfer molecule from the depot area (FIG. 6j) via a specific molecular handle. On retraction, the storage bond anchoring the transfer molecule to the depot surface ruptures and the transfer molecule now attached to the cantilever is moved to the target site. At a chosen position, the AFM stylus is lowered and the transfer molecule forms a deposition bond with an anchor molecule on the target surface. On retraction of the AFM stylus, the handle bond ruptures, leaving the transfer molecule attached to the target surface and the stylus free to pick up another transfer molecule from the depot area. SMCP is based on non-covalent but thermally stable bonds for storage (depot), handling (AFM stylus) and deposition (target)<sup>23</sup>. Anchors and handles are typically composed of DNA<sup>175,176</sup>, but alternatively, a broad range of protein-based ligand–receptor systems can be used. Anchors and handles must be chosen such that the force required to rupture the storage bond is lower than the force required to rupture the handle bond, which in turn is lower than the force required to rupture the deposition bond. Each of these steps is monitored by force–distance traces that can be read to determine whether

each step of the cut-and-paste assay occurs as expected<sup>177</sup>. Several thousand cycles may be carried out with negligible loss in transfer efficiency<sup>178</sup>. SMCP has been used to assemble recognition patterns based on either short DNA or RNA strands or proteins. When proteins are used, a force hierarchy must be chosen such that proteins are not denatured by forces they are subject to during transfer<sup>176</sup>. Larger biomolecules or nanoparticles have also been included in patterns assembled by SMCP<sup>178</sup>. In addition, split aptamers have been recombined locally to form functional receptors for small molecules<sup>179</sup>.

### AFM as a multifunctional toolbox

We have reviewed the unique capability of AFM-based technologies to image, probe, parameterize and manipulate biointerfaces. In some of these applications, especially when characterizing complex biosystems, it is advisable to complement AFM with optical microscopy and spectroscopy. In the following sections, we outline how AFM-based methods can be combined with other techniques to bring chemical, biophysical, and cell and molecular biological laboratories to the stylus. Based on selected examples, we summarize promising research highlights that we predict will pave the way for how AFM-based technologies are applied to address the current and future problems of biointerfaces.

### Combining advanced optical microscopy with AFM.

The combination of AFM with optical microscopy, including differential interference contrast or phase contrast microscopy, was introduced shortly after AFM. However, working with complex biointerfaces, such as living cells or tissues, often requires the correlation of topographical or mechanical properties measured by AFM with morphological information. Hence, fluorescence microscopy imaging of specifically labelled biomolecular species in living cells can be advantageous<sup>117,123,180</sup>. The resolution of optical microscopy should be as high as possible to be able to relate optical images with AFM images, which are not constrained by the diffraction limit. One promising way to close this resolution gap is to combine super-resolution microscopy with AFM<sup>181,182</sup>. AFM-based methods are particularly suitable to characterize single molecules at biointerfaces. Topographic, mechanical and physicochemical information can be correlated with single-molecule fluorescence techniques or with total internal reflection fluorescence (TIRF) microscopy, which provides an outstanding signal-to-noise ratio for the detection of fluorophores (FIG. 7a,b). Such combinations have been applied to optically monitor the cut-and-paste of single molecules<sup>177</sup>, to watch motor proteins walking<sup>183</sup> and to observe the extraction and rupture of membrane tethers from cell surfaces adhering to substrates<sup>117</sup>.

**AFM-based optical nanospectroscopy.** Most biointerfaces are composed of various different biological or chemical molecules. A ubiquitous example of such an interface is the plasma membrane that forms the surface of living cells. The membrane comprises thousands of different molecules (such as lipids, sugars and proteins),

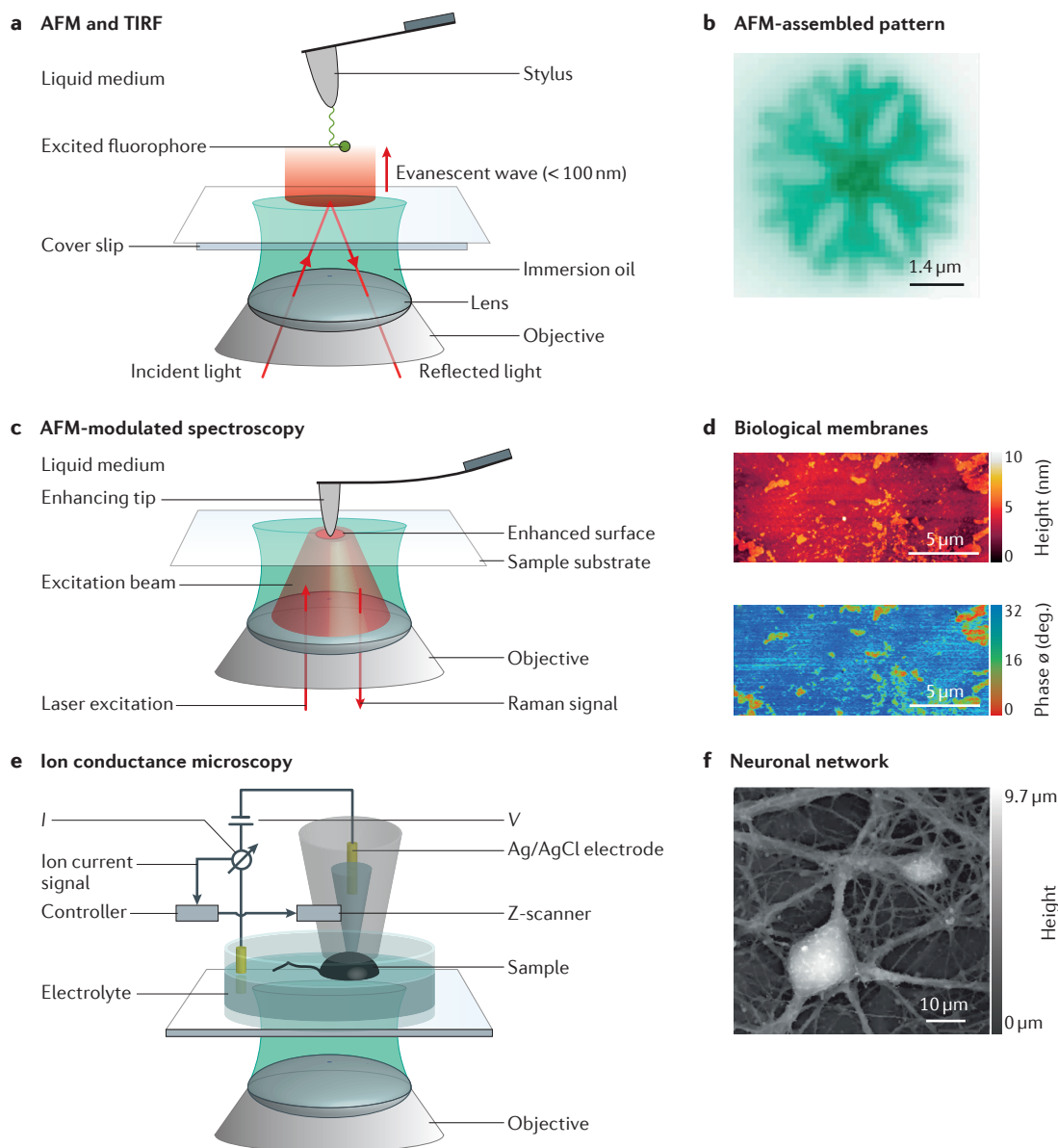


**Figure 7 | Combining AFM with other microscopic and spectroscopic approaches.** **a** | Schematic diagram of the combination of atomic force microscopy (AFM) and total internal reflection fluorescence (TIRF) microscopy. TIRF only detects fluorescence within the evanescent wave extending  $\sim 100$  nm into the solution. This restriction reduces background signal and improves the signal-to-noise ratio of fluorescence. **b** | A microscopic snowflake pattern deposited from 552 green fluorescent proteins (GFP) using the AFM-based cut-and-paste assay and imaged by TIRF. **c** | Principle of AFM-based tip enhanced or scattered spectroscopy. In tip-enhanced Raman spectroscopy (TERS), an objective focuses the excitation beam to the tip and sample to collect the Raman scattered light. Enhanced scattering only occurs where the tip is close to the sample. **d** | AFM topography (top) and the phase of the excitation resonance of the amide mode (bottom) of purple membrane patches. In this experiment, the AFM tip was used to contour the sample and to scatter infrared light from the tip-sample interface. **e** | Schematic diagram of scanning conductance microscopy (SCM). An electrolyte-filled nanopipette mounted on piezoelectric elements contours the surface of an object ( $I$ , current;  $V$ , voltage). **f** | Image of a hippocampal neuron showing the neuronal network. Panel **b** is reproduced with permission from REF. 176, American Chemical Society. Panel **d** is adapted with permission from REF. 185, American Chemical Society. Panel **f** is reproduced with permission from REF. 188, Macmillan Publishers Limited.

and its composition and supramolecular arrangement dynamically change in accordance with the cell state. Understanding this dynamic process requires structural and chemical analysis of all the components of cellular membranes across length scales ranging from sub-nanometre to micrometre and times scales ranging

from microseconds to hours. Although optical super-resolution microscopy has been developed and brought to nanometre-scale imaging, in complex environments, observation of a species of interest often requires selective labelling. Because fluorescence labelling can only be performed on a few molecules of interest at once

(up to about five species), most of the cellular membrane is not imaged. Apertureless scanning near-field optical microscopy (SNOM) can provide nanoscopic resolution of biointerfaces and can, in combination with label-free spectroscopic methods, analyse their chemical composition<sup>184</sup> (FIG. 7c). In such measurements, a sharp stylus contours the biointerface and at the same time acts as an optical antenna that confines incident electromagnetic waves to dimensions determined by the nanoscale tip apex, which enhances spectral emission at the interface. Together the topography and the spectral composition of the emitted light detected for each topographic pixel can provide insight into the chemical composition of the biointerface. Although this method is still in its infancy, recent progress indicates that it is possible to image membranes or other biointerfaces. Examples include using SNOM to topographically image purple membrane and at the same time detect local protein density via infrared radiation<sup>185</sup> (FIG. 7d). Others have applied the same principle but used infrared to differentiate native and misfolded protein aggregates<sup>186</sup>.

**Scanning ion conductance microscopy.** SICM raster scans an electrically charged micro- or nanopipette filled with electrolyte across a biointerface (FIG. 7e). As the distance between the tip of the micropipette and the sample changes, the ion conductance, and thus the current flowing through the tip–sample gap, also changes. Variations in the ion current are used as a feedback signal to keep the distance between the pipette and sample constant while contouring the biological object<sup>187</sup>. SICM has been refined over the years in various offsprings such as hopping probe ion conductance microscopy<sup>188,189</sup>. The broad applicability of SICM to characterize biointerfaces, ranging from neurons, stereocilia of hair cells, synapses, clathrin-coated pits or lung tissue, has been demonstrated<sup>190–192</sup> (FIG. 7f). On living cells, the topographic resolution can approach <10 nm, which is sufficient to localize single-membrane proteins<sup>193</sup>. In addition to contouring biointerfaces, the pipette can conduct local patch-clamp measurements for the electrophysiological characterization of presynaptic ion channels or neurotransmitter release<sup>189,190</sup>. Recently, SICM-based quantitative surface conductivity microscopy has been introduced, which contours biological membranes and simultaneously maps their surface charge density at nanoscale resolution<sup>194</sup>. The approach is sufficiently sensitive to differentiate the surface charge densities of cationic, anionic and zwitterionic lipids. Particularly, when combined with other AFM-based imaging modes — confocal microscopy or super-resolution optical microscopy<sup>195,196</sup> — SICM becomes a powerful tool for non-contact high-resolution imaging of the complex 3D surfaces of living cells.

### Summary and perspective

Since its invention 30 years ago, AFM has undoubtedly had a considerable impact in the life sciences and in characterizing and manipulating biological interfaces. In this Review, we have endeavoured to highlight the wealth of AFM-based modalities that have been implemented over the

years leading to the multiparametric and multifunctional characterization of biological systems.

AFM-based methods allow imaging of native biointerfaces at high resolution and simultaneous mapping of the mechanical, electrostatic, kinetic and thermodynamic properties of functional groups and binding sites. AFM-based force spectroscopic modes enable the characterization of single receptor–ligand bonds, protein unfolding and refolding, and the mechanoelastic properties of peptides, nucleic acids, sugars and polymers. Cell adhesion to the interface of substrates, other cells or tissues can also be quantified using such modes. AFM-based SPL methods allow the nanoscopic patterning of surfaces with proteins, lipids, polymers or chemical molecules. Advanced SPL methods even allow the hierarchical assembly of 3D biomolecular systems on interfaces. AFM-based microcantilevers are used to detect molecular binding and reactions at interfaces in real time. Examples include the binding of antibodies, complementary strands of nucleic acids and nanomechanical vibrations of cells, which are sensitive to drug treatment. In some highlighted examples, the future trend to combine different AFM-based approaches to characterize biointerfaces is already distinct. The combination of two or more AFM-based modalities to characterize multiple parameters of complex biointerfaces, of which FD-based AFM is a prominent example, increases the diversity and volume of data that can be acquired in an experiment. Such combination allows, for example, correlation of ligand-binding events to topographies of protein complexes or living cells. In other examples, AFM is combined with modern optical techniques such as confocal fluorescence microscopy or Raman spectroscopy. It is evident that these combinations provide new ways to unravel the structure–function relationship of complex biointerfaces and to modify these properties. We expect that in the near future more AFM-based modalities and complementary techniques will be combined into single experiments to address pertinent problems and challenges in the life sciences.

Challenges that might be addressed with multifunctional approaches, which focus and combine modern chemical, biophysical and cell biological laboratories on a nanoscopic stylus, include the characterization of the different functional states of the same cell-surface receptor depending on its location in the cell membrane and the determination of the interactions that modulate these states. How these states depend on the supramolecular assembly of receptors and how the living cell modulates these states are also open questions. Other challenges might be to use systems engineering approaches to guide chemical or biological reaction pathways by the hierarchical assembly of enzymes, polymers or cells on biointerfaces. Ultimately, manifold discoveries and engineering possibilities will materialize as multiparametric tools allow systems of increasing complexity to be probed and manipulated. It seems beyond doubt that AFM-based methods that revolutionized nanotechnology<sup>5</sup> are to have a similar effect on how we view and utilize biointerfaces.

1. Nel, A. E. *et al.* Understanding biophysicochemical interactions at the nano–bio interface. *Nat. Mater.* **8**, 543–557 (2009).
2. Ross, A. M. & Lahann, J. Current trends and challenges in biointerfaces science and engineering. *Annu. Rev. Chem. Biomol.* **6**, 161–186 (2015).
3. Stevens, M. M. & George, J. H. Exploring and engineering the cell surface interface. *Science* **310**, 1135–1138 (2005).
4. Andrews, R. N., Co, C. C. & Ho, C. C. Engineering dynamic biointerfaces. *Curr. Opin. Chem. Eng.* **11**, 28–33 (2016).
5. Gerber, C. & Lang, H. P. How the doors to the nanoworld were opened. *Nat. Nanotechnol.* **1**, 3–5 (2006).
6. Binnig, G., Quate, C. F. & Gerber, C. Atomic force microscope. *Phys. Rev. Lett.* **56**, 930–933 (1986). **This paper describes the invention of AFM.**
7. Drake, B. *et al.* Imaging crystals, polymers, and processes in water with the atomic force microscope. *Science* **243**, 1586–1589 (1989).
8. Radmacher, M., Tillmann, R. W., Fritz, M. & Gaub, H. E. From molecules to cells: imaging soft samples with the atomic force microscope. *Science* **257**, 1900–1905 (1992).
9. Garcia, R. & Herruzo, E. T. The emergence of multifrequency force microscopy. *Nat. Nanotechnol.* **7**, 217–226 (2012).
10. Ando, T., Uchihashi, T. & Kodera, N. High-speed AFM and applications to biomolecular systems. *Ann. Rev. Biophys.* **42**, 393–414 (2013).
11. Zhang, S., Aslan, H., Besenbacher, F. & Dong, M. Quantitative biomolecular imaging by dynamic nanomechanical mapping. *Chem. Soc. Rev.* **43**, 7412–7429 (2014).
12. Dufrene, Y. F. *et al.* Imaging modes of atomic force microscopy for application in molecular and cell biology. *Nat. Nanotechnol.* <http://dx.doi.org/10.1038/nnano.2017.45> (2017).
13. Frisbie, C. D., Rozsnyai, L. F., Noy, A., Wrighton, M. S. & Lieber, C. M. Functional group imaging by chemical force microscopy. *Science* **265**, 2071–2074 (1994).
14. Hinterdorfer, P. & Dufrene, Y. F. Detection and localization of single molecular recognition events using atomic force microscopy. *Nat. Methods* **3**, 347–355 (2006).
15. Müller, D. J., Helenius, J., Alsteens, D. & Dufrene, Y. F. Force probing surfaces of living cells to molecular resolution. *Nat. Chem. Biol.* **5**, 383–390 (2009).
16. Dufrene, Y. F., Martinez-Martin, D., Medalsy, I., Alsteens, D. & Müller, D. J. Multiparametric imaging of biological systems by force–distance curve-based AFM. *Nat. Methods* **10**, 847–854 (2013).
17. Lang, H. P. & Gerber, C. Microcantilever sensors. *Top. Curr. Chem.* **285**, 1–27 (2008).
18. Müller, D. J. & Dufrene, Y. F. Atomic force microscopy as a multifunctional molecular toolbox in nanobiotechnology. *Nat. Nanotechnol.* **3**, 261–269 (2008).
19. Pires, D. *et al.* Nanoscale three-dimensional patterning of molecular resists by scanning probes. *Science* **328**, 732–735 (2010).
20. Garcia, R., Knoll, A. W. & Riedo, E. Advanced scanning probe lithography. *Nat. Nanotechnol.* **9**, 577–587 (2014).
21. Puchner, E. M. & Gaub, H. E. Single-molecule mechanoenzymatics. *Ann. Rev. Biophys.* **41**, 497–518 (2012).
22. Cattin, C. J. *et al.* Mechanical control of mitotic progression in single animal cells. *Proc. Natl Acad. Sci. USA* **112**, 11258–11263 (2015).
23. Kufer, S. K., Puchner, E. M., Gump, H., Liedl, T. & Gaub, H. E. Single-molecule cut-and-paste surface assembly. *Science* **319**, 594–596 (2008).
24. Engel, A. & Müller, D. J. Observing single biomolecules at work with the atomic force microscope. *Nat. Struct. Biol.* **7**, 715–718 (2000).
25. Kuznetsov, Y. G. & McPherson, A. Atomic force microscopy in imaging of viruses and virus-infected cells. *Microbiol. Mol. Biol. Rev.* **75**, 268–285 (2011).
26. Ido, S. *et al.* Beyond the helix pitch: direct visualization of native DNA in aqueous solution. *ACS Nano* **7**, 1817–1822 (2013).
27. Pyne, A., Thompson, R., Leung, C., Roy, D. & Hoogenboom, B. W. Single-molecule reconstruction of oligonucleotide secondary structure by atomic force microscopy. *Small* **10**, 3257–3261 (2014).
28. Ido, S. *et al.* Immunoactive two-dimensional self-assembly of monoclonal antibodies in aqueous solution revealed by atomic force microscopy. *Nat. Mater.* **13**, 264–270 (2014).
29. Seelert, H. *et al.* Proton powered turbine of a plant motor. *Nature* **405**, 418–419 (2000).
30. Fotiadis, D. *et al.* Atomic-force microscopy: rhodopsin dimers in native disc membranes. *Nature* **421**, 127–128 (2003).
31. Uchihashi, T., Iino, R., Ando, T. & Noji, H. High-speed atomic force microscopy reveals rotary catalysis of rotorless F<sub>1</sub>-ATPase. *Science* **333**, 755–758 (2011).
32. Müller, D. J., Hand, G. M., Engel, A. & Sosinsky, G. Conformational changes in surface structures of isolated Connexin26 gap junctions. *EMBO J.* **21**, 3598–3607 (2002).
33. Müller, D. J. & Engel, A. Voltage and pH-induced channel closure of porin OmpF visualized by atomic force microscopy. *J. Mol. Biol.* **285**, 1347–1351 (1999).
34. Mari, S. A. *et al.* pH-induced conformational change of the beta-barrel-forming protein OmpG reconstituted into native *E. coli* lipids. *J. Mol. Biol.* **396**, 610–616 (2010).
35. Czajkowsky, D. M., Hotze, E. M., Shao, Z. & Tweten, R. K. Vertical collapse of a cytolysin prepore moves its transmembrane beta-hairpins to the membrane. *EMBO J.* **23**, 3206–3215 (2004).
36. Shibata, M., Uchihashi, T., Yamashita, H., Kandori, H. & Ando, T. Structural changes in bacteriorhodopsin in response to alternate illumination observed by high-speed atomic force microscopy. *Angew. Chem. Int. Ed.* **50**, 4410–4413 (2011).
37. Mari, S. A. *et al.* Gating of the MlotK1 potassium channel involves large rearrangements of the cyclic nucleotide-binding domains. *Proc. Natl Acad. Sci. USA* **108**, 20802–20807 (2011).
38. Rangel, M. *et al.* Real-time visualization of conformational changes within single MloK1 cyclic nucleotide-modulated channels. *Nat. Commun.* **7**, 12789 (2016).
39. Müller, D. J. *et al.* Observing membrane protein diffusion at subnanometer resolution. *J. Mol. Biol.* **327**, 925–930 (2003).
40. Karner, A. *et al.* Tuning membrane protein mobility by confinement into nanodomains. *Nat. Nanotechnol.* <http://dx.doi.org/10.1038/nnano.2016.236> (2016).
41. Kodera, N., Yamamoto, D., Ishikawa, R. & Ando, T. Video imaging of walking myosin V by high-speed atomic force microscopy. *Nature* **468**, 72–76 (2010). **This study describes single-motor proteins walking along actin filaments.**
42. Cisneros, D. A., Hung, C., Franz, C. M. & Müller, D. J. Observing growth steps of collagen self-assembly by time-lapse high-resolution atomic force microscopy. *J. Struct. Biol.* **154**, 232–245 (2006).
43. Stamo, D. R., Stock, E., Franz, C. M., Jahnke, T. & Haschke, H. Imaging collagen type I fibrillogenesis with high spatiotemporal resolution. *Ultramicroscopy* **149**, 86–94 (2015).
44. Lehto, T., Miaczynska, M., Zerial, M., Müller, D. J. & Severin, F. Observing the growth of individual actin filaments in cell extracts by time-lapse atomic force microscopy. *FEBS Lett.* **551**, 25–28 (2003).
45. Sharma, S. *et al.* Nanostructured self-assembly of inverted formin 2 (INF2) and F-actin-INF2 complexes revealed by atomic force microscopy. *Langmuir* **30**, 7533–7539 (2014).
46. Friedrichs, J., Taubenberger, A., Franz, C. M. & Müller, D. J. Cellular remodelling of individual collagen fibrils visualized by time-lapse AFM. *J. Mol. Biol.* **372**, 594–607 (2007).
47. Gudzenko, T. & Franz, C. M. Studying early stages of fibronectin fibrillogenesis in living cells by atomic force microscopy. *Mol. Biol. Cell* **26**, 3190–3204 (2015).
48. Stark, M., Stark, R. W., Heckl, W. M. & Guckenberger, R. Inverting dynamic force microscopy: from signals to time-resolved interaction forces. *Proc. Natl Acad. Sci. USA* **99**, 8473–8478 (2002).
49. Martinez-Martin, D., Herruzo, E. T., Dietz, C., Gomez-Herrero, J. & Garcia, R. Noninvasive protein structural flexibility mapping by bimodal dynamic force microscopy. *Phys. Rev. Lett.* **106**, 198101 (2011).
50. Raman, A. *et al.* Mapping nanomechanical properties of live cells using multi-harmonic atomic force microscopy. *Nat. Nanotechnol.* **6**, 809–814 (2011).
51. Hansma, P. K., Schitter, G., Fantner, G. E. & Prater, C. High-speed atomic force microscopy. *Science* **314**, 601–602 (2006).
52. Fantner, G. E. *et al.* Components for high speed atomic force microscopy. *Ultramicroscopy* **106**, 881–887 (2006).
53. Viani, M. B. *et al.* Probing protein–protein interactions in real time. *Nat. Struct. Biol.* **7**, 644–647 (2000).
54. Watanabe-Nakayama, T., Itami, M., Kodera, N., Ando, T. & Konno, H. High-speed atomic force microscopy reveals strongly polarized movement of clostridial collagenase along collagen fibrils. *Sci. Rep.* **6**, 28975 (2016).
55. Chiaruttini, N. *et al.* Relaxation of loaded ESCRTIII spiral springs drives membrane deformation. *Cell* **163**, 866–879 (2015).
56. Yamashita, H. *et al.* Single-molecule imaging on living bacterial cell surface by high-speed AFM. *J. Mol. Biol.* **422**, 300–309 (2012).
57. Sakiyama, Y., Mazur, A., Kapinos, L. E. & Lim, R. Y. Spatiotemporal dynamics of the nuclear pore complex transport barrier resolved by high-speed atomic force microscopy. *Nat. Nanotechnol.* **11**, 719–725 (2016).
58. Butt, H. J., Cappella, B. & Kappl, M. Force measurements with the atomic force microscope: technique, interpretation and applications. *Surf. Sci. Rep.* **59**, 1–152 (2005).
59. Ducker, W. A., Senden, T. J. & Pashley, R. M. Direct measurement of colloidal forces using an atomic force microscope. *Nature* **353**, 239–241 (1991).
60. Pelling, A. E., Sehati, S., Gralla, E. B., Valentine, J. S. & Gimzewski, J. K. Local nanomechanical motion of the cell wall of *Saccharomyces cerevisiae*. *Science* **305**, 1147–1150 (2004).
61. Krieg, M., Dunn, A. R. & Goodman, M. B. Mechanical control of the sense of touch by beta-spectrin. *Nat. Cell Biol.* **16**, 224–233 (2014).
62. Vasquez, V., Krieg, M., Lockhead, D. & Goodman, M. B. Phospholipids that contain polyunsaturated fatty acids enhance neuronal cell mechanics and touch sensation. *Cell Rep.* **6**, 70–80 (2014).
63. Krieg, M. *et al.* Tensile forces govern germ-layer organization in zebrafish. *Nat. Cell Biol.* **10**, 429–436 (2008). **This study uses AFM to settle a long-standing dispute regarding whether it is cell adhesion or cortex tension that is responsible for cell sorting in the developing zebrafish embryo.**
64. Strilic, B. *et al.* Electrostatic cell-surface repulsion initiates lumen formation in developing blood vessels. *Curr. Biol.* **20**, 2003–2009 (2010).
65. Matzke, R., Jacobson, K. & Radmacher, M. Direct, high-resolution measurement of furrow stiffening during division of adherent cells. *Nat. Cell Biol.* **3**, 607–610 (2001).
66. Stewart, M. P. *et al.* Hydrostatic pressure and the actomyosin cortex drive mitotic cell rounding. *Nature* **469**, 226–230 (2011).
67. Cross, S. E., Jin, Y. S., Rao, J. & Gimzewski, J. K. Nanomechanical analysis of cells from cancer patients. *Nat. Nanotechnol.* **2**, 780–783 (2007).
68. Iyer, S., Gaikwad, R. M., Subba-Rao, V., Woodworth, C. D. & Sokolov, I. Atomic force microscopy detects differences in the surface brush of normal and cancerous cells. *Nat. Nanotechnol.* **4**, 389–393 (2009).
69. Martinez-Martin, D. *et al.* Resolving structure and mechanical properties at the nanoscale of viruses with frequency modulation atomic force microscopy. *PLoS ONE* **7**, e30204 (2012).
70. Roos, W. H. *et al.* Mechanics of bacteriophage maturation. *Proc. Natl Acad. Sci. USA* **109**, 2342–2347 (2012).
71. Marchetti, M., Wuite, G. & Roos, W. H. Atomic force microscopy observation and characterization of single virions and virus-like particles by nano-indentation. *Curr. Opin. Virol.* **18**, 82–88 (2016).
72. Janmey, P. A., Georges, P. C. & Hvidt, S. Basic rheology for biologists. *Methods Cell Biol.* **83**, 3–27 (2007).
73. Nawaz, S. *et al.* Cell visco-elasticity measured with AFM and optical trapping at sub-micrometer deformations. *PLoS ONE* **7**, e45297 (2012).
74. Medalsy, I. D. & Müller, D. J. Nanomechanical properties of proteins and membranes depend on loading rate and electrostatic interactions. *ACS Nano* **7**, 2642–2650 (2013).
75. Herruzo, E. T., Perrino, A. P. & Garcia, R. Fast nanomechanical spectroscopy of soft matter. *Nat. Commun.* **5**, 3126 (2014).
76. Stewart, M. P. *et al.* Wedged AFM-cantilevers for parallel plate cell mechanics. *Methods* **60**, 186–194 (2013).
77. Fischer-Friedrich, E., Hyman, A. A., Julicher, F., Müller, D. J. & Helenius, J. Quantification of surface tension and internal pressure generated by single mitotic cells. *Sci. Rep.* **4**, 6213 (2014).

78. Fischer-Friedrich, E. *et al.* Rheology of the active cell cortex in mitosis. *Biophys. J.* **111**, 589–600 (2016).
79. Lee, G. U., Kidwell, D. A. & Colton, R. J. Sensing discrete streptavidin–biotin interactions with atomic force microscopy. *Langmuir* **10**, 354–357 (1994).
80. Moy, V. T., Florin, E. L. & Gaub, H. E. Intermolecular forces and energies between ligands and receptors. *Science* **266**, 257–259 (1994).
81. Baumann, F., Heucke, S. F., Pippig, D. A. & Gaub, H. E. Tip localization of an atomic force microscope in transmission microscopy with nanoscale precision. *Rev. Sci. Instrum.* **86**, 035109 (2015).
82. Evans, E. A. & Calderwood, D. A. Forces and bond dynamics in cell adhesion. *Science* **316**, 1148–1153 (2007).
83. Dudko, O. K., Hummer, G. & Szabo, A. Theory, analysis, and interpretation of single-molecule force spectroscopy experiments. *Proc. Natl Acad. Sci. USA* **105**, 15755–15760 (2008).
84. Fridtle, R. W., Noy, A. & De Yoreo, J. J. Interpreting the widespread nonlinear force spectra of intermolecular bonds. *Proc. Natl Acad. Sci. USA* **109**, 13573–13578 (2012).
85. Woodside, M. T. & Block, S. M. Reconstructing folding energy landscapes by single-molecule force spectroscopy. *Ann. Rev. Biophys. Chem.* **43**, 19–39 (2014).
86. Perez-Jimenez, R. *et al.* Single-molecule paleoenzymology probes the chemistry of resurrected enzymes. *Nat. Struct. Mol. Biol.* **18**, 592–596 (2011).
87. Oberhauser, A. F., Hansma, P. K., Carrion-Vazquez, M. & Fernandez, J. M. Stepwise unfolding of titin under force-clamp atomic force microscopy. *Proc. Natl Acad. Sci. USA* **98**, 468–472 (2001).
88. Stahl, S. W., Puchner, E. M. & Gaub, H. E. Photothermal cantilever actuation for fast single-molecule force spectroscopy. *Rev. Sci. Instrum.* **80**, 073702 (2009).
89. Krieg, M., Helenius, J., Heisenberg, C. P. & Müller, D. J. A bond for a lifetime: employing membrane nanotubes from living cells to determine receptor–ligand kinetics. *Angew. Chem. Int. Ed.* **47**, 9775–9777 (2008).
90. Alsteens, D. *et al.* Imaging G protein-coupled receptors while quantifying their ligand-binding free-energy landscape. *Nat. Methods* **12**, 845–851 (2015).
91. Wildling, L. *et al.* Probing binding pocket of serotonin transporter by single molecular force spectroscopy on living cells. *J. Biol. Chem.* **287**, 105–113 (2012).
92. Friedrichs, J., Helenius, J. & Müller, D. J. Quantifying cellular adhesion to extracellular matrix components by single-cell force spectroscopy. *Nat. Protoc.* **5**, 1353–1361 (2010).
93. Schoeler, C. *et al.* Mapping mechanical force propagation through biomolecular complexes. *Nano Lett.* **15**, 7370–7376 (2015).
94. Sieben, C. *et al.* Influenza virus binds its host cell using multiple dynamic interactions. *Proc. Natl Acad. Sci. USA* **109**, 13626–13631 (2012).
95. Alsteens, D. *et al.* Nanomechanical mapping of first binding steps of a virus to animal cells. *Nat. Nanotechnol.* **12**, 177–183 (2017). **This paper maps virus-binding events on animal cells and simultaneously extracts the steps and free energy landscape of viral ligands binding to cell surface receptors.**
96. King, G. M., Carter, A. R., Churnside, A. B., Eberle, L. S. & Perkins, T. T. Ultrafast atomic force microscopy: atomic-scale stability and registration in ambient conditions. *Nano Lett.* **9**, 1451–1456 (2009).
97. Bull, M. S., Sullan, R. M., Li, H. & Perkins, T. T. Improved single molecule force spectroscopy using microfabricated cantilevers. *ACS Nano* **8**, 4984–4995 (2014).
98. Rief, M., Gautel, M., Oesterhelt, F., Fernandez, J. M. & Gaub, H. E. Reversible unfolding of individual titin immunoglobulin domains by AFM. *Science* **276**, 1109–1112 (1997). **This paper characterizes the mechanically induced unfolding and reversible refolding of single protein domains using AFM-based SMFS.**
99. Bippes, C. A. & Müller, D. J. High-resolution atomic force microscopy and spectroscopy of native membrane proteins. *Rep. Prog. Phys.* **74**, 086601 (2011).
100. Puchner, E. M. & Gaub, H. E. Force and function: probing proteins with AFM-based force spectroscopy. *Curr. Opin. Struct. Biol.* **19**, 605–614 (2009).
101. Žoldák, G. & Rief, M. Force as a single molecule probe of multidimensional protein energy landscapes. *Curr. Opin. Struct. Biol.* **23**, 48–57 (2013).
102. Kawamura, S., Colozo, A. T., Ge, L., Müller, D. J. & Park, P. S. Structural, energetic, and mechanical perturbations in rhodopsin mutant that causes congenital stationary night blindness. *J. Biol. Chem.* **287**, 21826–21835 (2012).
103. Mashaghi, A. *et al.* Reshaping of the conformational search of a protein by the chaperone trigger factor. *Nature* **500**, 98–101 (2013).
104. Nunes, J. M., Mayer-Hartl, M., Hartl, F. U. & Müller, D. J. Action of the Hsp70 chaperone system observed with single proteins. *Nat. Commun.* **6**, 6307 (2015).
105. Park, P. S. *et al.* Stabilizing effect of Zn<sup>2+</sup> in native bovine rhodopsin. *J. Biol. Chem.* **282**, 11377–11385 (2007).
106. Oesterhelt, F. *et al.* Unfolding pathways of individual bacteriorhodopsins. *Science* **288**, 143–146 (2000). **This paper describes the mechanically induced stepwise unfolding of membrane proteins using AFM-based SMFS.**
107. Damaghi, M., Koster, S., Bippes, C. A., Yildiz, O. & Müller, D. J. One  $\beta$ -hairpin follows the other: exploring refolding pathways and kinetics of the transmembrane  $\beta$ -barrel protein OmpG. *Angew. Chem. Int. Ed.* **50**, 7422–7424 (2011).
108. Kessler, M., Gottschalk, K. E., Janovjak, H., Müller, D. J. & Gaub, H. E. Bacteriorhodopsin folds into the membrane against an external force. *J. Mol. Biol.* **357**, 644–654 (2006).
109. Thoma, J., Bosshart, P., Pfreundschuh, M. & Müller, D. J. Out but not in: the large transmembrane  $\beta$ -barrel protein FhuA unfolds but cannot refold via  $\beta$ -hairpins. *Structure* **20**, 2185–2190 (2012).
110. Serdiuk, T. *et al.* YidC assists the stepwise and stochastic folding of membrane proteins. *Nat. Chem. Biol.* **12**, 911–917 (2016).
111. Thoma, J., Burmann, B. M., Hiller, S. & Müller, D. J. Impact of holdase chaperones Skp and SurA on the folding of beta-barrel outer-membrane proteins. *Nat. Struct. Mol. Biol.* **22**, 795–802 (2015).
112. Struckmeier, J. *et al.* Fully automated single-molecule force spectroscopy for screening applications. *Nanotechnology* **19**, 384020 (2008).
113. Otten, M. *et al.* From genes to protein mechanics on a chip. *Nat. Methods* **11**, 1127–1130 (2014).
114. Friedrichs, J. *et al.* A practical guide to quantify cell adhesion using single-cell force spectroscopy. *Methods* **60**, 169–178 (2013).
115. Benoit, M., Gabriel, D., Gerisch, G. & Gaub, H. E. Discrete interactions in cell adhesion measured by single-molecule force spectroscopy. *Nat. Cell Biol.* **2**, 313–317 (2000). **This paper introduces AFM-based force spectroscopy to quantify the adhesive forces established by living cells.**
116. Ulrich, F. *et al.* Wnt11 functions in gastrulation by controlling cell cohesion through Rab5c and E-cadherin. *Dev. Cell* **9**, 555–564 (2005).
117. Te Riet, J. *et al.* Dynamic coupling of ALCAM to the actin cortex strengthens cell adhesion to CD6. *J. Cell Sci.* **127**, 1595–1606 (2014).
118. Alsteens, D., Van Dijk, P., Lipke, P. N. & Dufreñe, Y. F. Quantifying the forces driving cell–cell adhesion in a fungal pathogen. *Langmuir* **29**, 13473–13480 (2013).
119. Beaussart, A. *et al.* Single-cell force spectroscopy of probiotic bacteria. *Biophys. J.* **104**, 1886–1892 (2013).
120. Friedrichs, J., Helenius, J. & Müller, D. J. Stimulated single-cell force spectroscopy to quantify cell adhesion receptor cross-talk. *Proteomics* **10**, 1455–1462 (2010).
121. Chaudhuri, O., Parekh, S. H., Lam, W. A. & Fletcher, D. A. Combined atomic force microscopy and side-view optical imaging for mechanical studies of cells. *Nat. Methods* **6**, 385–387 (2009).
122. Gonnermann, C. *et al.* Quantitating membrane bleb stiffness using AFM force spectroscopy and an optical sideview setup. *Integr. Biol. (Camb.)* **7**, 356–363 (2015).
123. Ramanathan, S. P. *et al.* Cdk1-dependent mitotic enrichment of cortical myosin II promotes cell rounding against confinement. *Nat. Cell Biol.* **17**, 148–159 (2015).
124. Rouven Bruckner, B., Pietuch, A., Nehls, S., Rother, J. & Janshoff, A. Ezrin is a major regulator of membrane tension in epithelial cells. *Sci. Rep.* **5**, 14700 (2015).
125. Heu, C., Berquand, A., Elie-Caille, C. & Nicod, L. Glycosate-induced stiffening of HaCaT keratinocytes, a Peak Force Tapping study on living cells. *J. Struct. Biol.* **178**, 1–7 (2012).
126. Hecht, F. M. *et al.* Imaging viscoelastic properties of live cells by AFM: power-law rheology on the nanoscale. *Soft Matter* **11**, 4584–4591 (2015).
127. Formosa-Dague, C., Speziale, P., Foster, T. J., Geoghegan, J. A. & Dufreñe, Y. F. Zinc-dependent mechanical properties of *Staphylococcus aureus* biofilm-forming surface protein SasG. *Proc. Natl Acad. Sci. USA* **113**, 410–415 (2016).
128. Beaussart, A., El-Kirat-Chatel, S., Fontaine, T., Latge, J. P. & Dufreñe, Y. F. Nanoscale biophysical properties of the cell surface galactosaminogalactan from the fungal pathogen *Aspergillus fumigatus*. *Nanoscale* **7**, 14996–15004 (2015).
129. Dong, M., Husale, S. & Sahin, O. Determination of protein structural flexibility by microsecond force spectroscopy. *Nat. Nanotechnol.* **4**, 514–517 (2009).
130. Medalsy, I., Hensen, U. & Müller, D. J. Imaging and quantifying chemical and physical properties of native proteins at molecular resolution by force–volume AFM. *Angew. Chem. Int. Ed.* **50**, 12103–12108 (2011).
131. Wegmann, S., Medalsy, I. D., Mandelkow, E. & Müller, D. J. The fuzzy coat of pathological human Tau fibrils is a two-layered polyelectrolyte brush. *Proc. Natl Acad. Sci. USA* **110**, E313–E321 (2013).
132. Zhang, S. *et al.* Coexistence of ribbon and helical fibrils originating from hIAPP[20–29] revealed by quantitative nanomechanical atomic force microscopy. *Proc. Natl Acad. Sci. USA* **110**, 2798–2803 (2013).
133. Grandbois, M., Dettmann, W., Benoit, M. & Gaub, H. E. Affinity imaging of red blood cells using an atomic force microscope. *J. Histochem. Cytochem.* **48**, 719–724 (2000).
134. Dague, E. *et al.* Chemical force microscopy of single live cells. *Nano Lett.* **7**, 3026–3030 (2007).
135. Dupres, V. *et al.* The yeast Wsc1 cell surface sensor behaves like a nanospring *in vivo*. *Nat. Chem. Biol.* **5**, 857–862 (2009).
136. Guo, S. F. *et al.* Measuring protein isoelectric points by AFM-based force spectroscopy using trace amounts of sample. *Nat. Nanotechnol.* **11**, 817–823 (2016).
137. Pfreundschuh, M., Hensen, U. & Müller, D. J. Quantitative imaging of the electrostatic field and potential generated by a transmembrane protein pore at subnanometer resolution. *Nano Lett.* **13**, 5585–5593 (2013).
138. Alsteens, D., Trabelsi, H., Soumillon, P. & Dufreñe, Y. F. Multiparametric atomic force microscopy imaging of single bacteriophages extruding from living bacteria. *Nat. Commun.* **4**, 2926 (2013).
139. Pfreundschuh, M. *et al.* Identifying and quantifying two ligand-binding sites while imaging native human membrane receptors by AFM. *Nat. Commun.* **6**, 8857 (2015).
140. Pfreundschuh, M., Alsteens, D., Hilbert, M., Steinmetz, M. O. & Müller, D. J. Localizing chemical groups while imaging single native proteins by high-resolution atomic force microscopy. *Nano Lett.* **14**, 2957–2964 (2014).
141. Kim, D. & Sahin, O. Imaging and three-dimensional reconstruction of chemical groups inside a protein complex using atomic force microscopy. *Nat. Nanotechnol.* **10**, 264–269 (2015).
142. Dong, M. & Sahin, O. A nanomechanical interface to rapid single-molecule interactions. *Nat. Commun.* **2**, 247 (2011).
143. Thomas, W. E., Vogel, V. & Sokurenko, E. Biophysics of catch bonds. *Ann. Rev. Biophys.* **37**, 399–416 (2008).
144. Janovjak, H., Struckmeier, J. & Müller, D. J. Hydrodynamic effects in fast AFM single-molecule force measurements. *Eur. Biophys. J.* **34**, 91–96 (2005).
145. Amo, C. A. & Garcia, R. Fundamental high-speed limits in single-molecule, single-cell, and nanoscale force spectroscopies. *ACS Nano* **10**, 7117–7124 (2016).
146. Rico, F., Gonzalez, L., Casuso, I., Puig-Vidal, M. & Scheuring, S. High-speed force spectroscopy unfolds titin at the velocity of molecular dynamics simulations. *Science* **342**, 741–743 (2013).
147. Fritz, J. *et al.* Translating biomolecular recognition into nanomechanics. *Science* **288**, 316–318 (2000). **This study introduces the use of microcantilevers to sense biomolecular binding.**
148. McKendry, R. *et al.* Multiple label-free biodetection and quantitative DNA-binding assays on a nanomechanical cantilever array. *Proc. Natl Acad. Sci. USA* **99**, 9783–9788 (2002).
149. Zhang, J. *et al.* Rapid and label-free nanomechanical detection of biomarker transcripts in human RNA. *Nat. Nanotechnol.* **1**, 214–220 (2006).
150. Braun, T. *et al.* Quantitative time-resolved measurement of membrane protein–ligand interactions using microcantilever array sensors. *Nat. Nanotechnol.* **4**, 179–185 (2009).

151. Ndieyira, J. W. *et al.* Surface-stress sensors for rapid and ultrasensitive detection of active free drugs in human serum. *Nat. Nanotechnol.* **9**, 225–232 (2014).
152. Patil, S. B. *et al.* Decoupling competing surface binding kinetics and reconfiguration of receptor footprint for ultrasensitive stress assays. *Nat. Nanotechnol.* **10**, 899–907 (2015).
153. Huber, F., Lang, H. P., Backmann, N., Rimoldi, D. & Gerber, C. Direct detection of a BRAF mutation in total RNA from melanoma cells using cantilever arrays. *Nat. Nanotechnol.* **8**, 125–129 (2013).
154. Huber, F. *et al.* Fast diagnostics of BRAF mutations in biopsies from malignant melanoma. *Nano Lett.* **16**, 5373–5377 (2016).
155. Barnes, J. R., Stephenson, R. J., Welland, M. E., Gerber, C. & Gimzewski, J. K. Photothermal spectroscopy with femtojoule sensitivity using a micromechanical device. *Nature* **372**, 79–81 (1994).
156. Kasas, S. *et al.* Detecting nanoscale vibrations as signature of life. *Proc. Natl Acad. Sci. USA* **112**, 378–381 (2015).
157. Carbonell, C. & Braunschweig, A. B. Toward 4D nanoprinting with tip-induced organic surface reactions. *Acc. Chem. Res.* <http://dx.doi.org/10.1021/acs.accounts.6b00307> (2016).
158. Tinazli, A., Piehler, J., Beuttler, M., Guckenberger, R. & Tampe, R. Native protein nanolithography that can write, read and erase. *Nat. Nanotechnol.* **2**, 220–225 (2007).
159. Martinez, R. V. *et al.* Large-scale nanopatterning of single proteins used as carriers of magnetic nanoparticles. *Adv. Mater.* **22**, 588–591 (2010).
160. Felts, J. R., Onses, M. S., Rogers, J. A. & King, W. P. Nanometer scale alignment of block-copolymer domains by means of a scanning probe tip. *Adv. Mater.* **26**, 2999–3002 (2014).
161. Shi, J., Chen, J. & Cremer, P. S. Sub-100 nm patterning of supported bilayers by nanoshaving lithography. *J. Am. Chem. Soc.* **130**, 2718–2719 (2008).
162. Cisneros, D. A., Friedrichs, J., Taubenberger, A., Franz, C. M. & Müller, D. J. Creating ultrathin nanoscopic collagen matrices for biological and biotechnological applications. *Small* **3**, 956–963 (2007).
163. Szoszkiewicz, R. *et al.* High-speed, sub-15 nm feature size thermochemical nanolithography. *Nano Lett.* **7**, 1064–1069 (2007).
164. Paul, P. C., Knoll, A. W., Holzner, F., Despont, M. & Duerig, U. Rapid turnaround scanning probe nanolithography. *Nanotechnology* **22**, 275306 (2011).
165. Gotsmann, B., Duerig, U., Frommer, J. & Hawker, C. J. Exploiting chemical switching in a Diels–Alder polymer for nanoscale probe lithography and data storage. *Adv. Funct. Mater.* **16**, 1499–1505 (2006).
166. Milner, A. A., Zhang, K. & Prior, Y. Floating tip nanolithography. *Nano Lett.* **8**, 2017–2022 (2008).
167. Carroll, K. M. *et al.* Fabricating nanoscale chemical gradients with ThermoChemical NanoLithography. *Langmuir* **29**, 8675–8682 (2013).
168. Jäschke, M. *et al.* The atomic force microscope as a tool to study and manipulate local surface properties. *Biosens. Bioelectron.* **11**, 601–612 (1996).
169. Salaita, K., Wang, Y. & Mirkin, C. A. Applications of dip-pen nanolithography. *Nat. Nanotechnol.* **2**, 145–155 (2007).
170. Lenhart, S., Mirkin, C. A. & Fuchs, H. *In situ* lipid dip-pen nanolithography under water. *Scanning* **32**, 15–23 (2010).
171. Kim, K. H., Moldovan, N. & Espinosa, H. D. A nanofountain probe with sub-100 nm molecular writing resolution. *Small* **1**, 632–635 (2005).
172. Onses, M. S. *et al.* Hierarchical patterns of three-dimensional block-copolymer films formed by electrohydrodynamic jet printing and self-assembly. *Nat. Nanotechnol.* **8**, 667–675 (2013).
173. Lenhart, S. *et al.* Lipid multilayer gratings. *Nat. Nanotechnol.* **5**, 275–279 (2010).
174. Huo, F. *et al.* Polymer pen lithography. *Science* **321**, 1658–1660 (2008).
175. Albrecht, C. *et al.* DNA: a programmable force sensor. *Science* **301**, 367–370 (2003).
176. Pippig, D. A., Baumann, F., Strackharn, M., Aschenbrenner, D. & Gaub, H. E. Protein–DNA chimeras for nano assembly. *ACS Nano* **8**, 6551–6555 (2014).
177. Kufer, S. K. *et al.* Optically monitoring the mechanical assembly of single molecules. *Nat. Nanotechnol.* **4**, 45–49 (2009).
178. Puchner, E. M., Kufer, S. K., Strackharn, M., Stahl, S. W. & Gaub, H. E. Nanoparticle self-assembly on a DNA-scaffold written by single-molecule cut-and-paste. *Nano Lett.* **8**, 3692–3695 (2008).
179. Strackharn, M., Stahl, S. W., Puchner, E. M. & Gaub, H. E. Functional assembly of aptamer binding sites by single-molecule cut-and-paste. *Nano Lett.* **12**, 2425–2428 (2012).
180. Franz, C. M. & Müller, D. J. Analysing focal adhesion structure by AFM. *J. Cell Sci.* **118**, 5315–5323 (2005).
181. Cordes, T. *et al.* Resolving single-molecule assembled patterns with superresolution blink-microscopy. *Nano Lett.* **10**, 645–651 (2010).
182. Monserrate, A., Casado, S. & Flors, C. Correlative atomic force microscopy and localization-based super-resolution microscopy: revealing labelling and image reconstruction artefacts. *Chemphyschem* **15**, 647–650 (2014).
183. Fukuda, S. *et al.* High-speed atomic force microscope combined with single-molecule fluorescence microscopy. *Rev. Sci. Instrum.* **84**, 073706 (2013).
184. Schmid, T., Opilik, L., Blum, C. & Zenobi, R. Nanoscale chemical imaging using tip-enhanced Raman spectroscopy: a critical review. *Angew. Chem. Int. Ed.* **52**, 5940–5954 (2013).
185. Berweger, S. *et al.* Nano-chemical infrared imaging of membrane proteins in lipid bilayers. *J. Am. Chem. Soc.* **135**, 18292–18295 (2013).
186. Ruggeri, F. S. *et al.* Infrared nanospectroscopy characterization of oligomeric and fibrillar aggregates during amyloid formation. *Nat. Commun.* **6**, 7831 (2015).
187. Hansma, P. K., Drake, B., Marti, O., Gould, S. A. & Prater, C. B. The scanning ion-conductance microscope. *Science* **243**, 641–643 (1989).
- This classic study describes the invention of scanning ion conductance microscopy.**
188. Novak, P. *et al.* Nanoscale live-cell imaging using hopping probe ion conductance microscopy. *Nat. Methods* **6**, 279–281 (2009).
189. Novak, P. *et al.* Nanoscale-targeted patch-clamp recordings of functional presynaptic ion channels. *Neuron* **79**, 1067–1077 (2013).
190. Takahashi, Y. *et al.* Multifunctional nanoprobe for nanoscale chemical imaging and localized chemical delivery at surfaces and interfaces. *Angew. Chem. Int. Ed.* **50**, 9638–9642 (2011).
191. Shevchuk, A. I. *et al.* An alternative mechanism of clathrin-coated pit closure revealed by ion conductance microscopy. *J. Cell Biol.* **197**, 499–508 (2012).
192. Novak, P. *et al.* Imaging single nanoparticle interactions with human lung cells using fast ion conductance microscopy. *Nano Lett.* **14**, 1202–1207 (2014).
193. Shevchuk, A. I. *et al.* Imaging proteins in membranes of living cells by high-resolution scanning ion conductance microscopy. *Angew. Chem. Int. Ed.* **45**, 2212–2216 (2006).
194. Klausen, L. H., Fuhs, T. & Dong, M. Mapping surface charge density of lipid bilayers by quantitative surface conductivity microscopy. *Nat. Commun.* **7**, 12447 (2016).
195. Ossola, D. *et al.* Simultaneous scanning ion conductance microscopy and atomic force microscopy with microchanneled cantilevers. *Phys. Rev. Lett.* **115**, 238103 (2015).
196. Leo-Macias, A. *et al.* Nanoscale visualization of functional adhesion/excitability nodes at the intercalated disc. *Nat. Commun.* **7**, 10342 (2016).
197. Galvagnion, C. *et al.* Lipid vesicles trigger alpha-synuclein aggregation by stimulating primary nucleation. *Nat. Chem. Biol.* **11**, 229–234 (2015).
198. Lind, T. K., Zielinska, P., Wacklin, H. P., Urbanczyk-Lipkowska, Z. & Cardenas, M. Continuous flow atomic force microscopy imaging reveals fluidity and time-dependent interactions of antimicrobial dendrimer with model lipid membranes. *ACS Nano* **8**, 396–408 (2014).
199. Ko, S. H. *et al.* Synergistic self-assembly of RNA and DNA molecules. *Nat. Chem.* **2**, 1050–1055 (2010).
200. Sapro, K. T. *et al.* One beta hairpin after the other: exploring mechanical unfolding pathways of the transmembrane beta-barrel protein OmpG. *Angew. Chem. Int. Ed.* **48**, 8306–8308 (2009).
201. Strackharn, M., Pippig, D. A., Meyer, P., Stahl, S. W. & Gaub, H. E. Nanoscale arrangement of proteins by single-molecule cut-and-paste. *J. Am. Chem. Soc.* **134**, 15193–15196 (2012).

#### Acknowledgements

D.A. was supported by the Belgian National Foundation for Scientific Research (FNRS) and the Université catholique de Louvain (Fonds Spéciaux de Recherche). D.A. is a Research Associate FNRS. D.J.M. was supported by the Swiss National Science Foundation (SNF; grant 310030B\_160225) and the NCCR Molecular Systems Engineering. C.G. and D.J.M. were supported by the Swiss Nanoscience Institute. H.E.G. acknowledges financial support by the ERC grant CelluFuel.

#### Competing interests statement

The authors declare no competing interests.

#### How to cite this article

Alsteens, D. *et al.* Atomic force microscopy-based characterization and design of biointerfaces. *Nat. Rev. Mater.* **2**, 17008 (2017).